2010

Positron autoradiography for intravascular vulnerable plaque imaging

Peter Petrek
Louisiana State University and Agricultural and Mechanical College, ppetrek@gmail.com

POSITRON AUTORADIOGRAPHY FOR INTRAVASCULAR VULNERABLE PLAQUE IMAGING

A Thesis

Submitted to the Graduate faculty of the
Louisiana State University and
Agricultural and Mechanical College
in Partial Fulfillment of the
Requirements for the Degree of
Master of Science

in

The Department of Physics and Astronomy

by
Peter Petrek
B.A., Augustana College 2005
May, 2010

ACKNOWLEDGMENTS

I extend my thanks to my committee chair, Dr. Polad Shikhaliev, for all his advice and help in research and preparation of this thesis and to all of the members of my supervisory committee: Dr. Kip Matthews, Dr. Ken Hogstrom, and Dr. Greg Stacy for their assistance and taking time to serve on my supervisory committee. I also thank Shannon Fritz for her selfless help with every aspect of the research project. When it came to the project everyone was willing to think outside the box and provide suggestions to improve the outcome of the project, while maintain a positive attitude.

Finally, I thank the staff at LSU and Mary Bird Perkins Cancer Center for all their help. This project was supported by NIH grant R21E006142 (Dr. Shikhaliev PI).

TABLE OF CONTENTS

LIST OF FIGURES

ABSTRACT

Purpose: To develop and investigate an intravascular storage phosphor detector for imaging and detection of vulnerable coronary artery plaques.

Methods: The concept of the detection of vulnerable plaques (i.e., plaques with inflammation) is based on accumulation of fluorodeoxyglucose (FDG) in inflammation sites. The FDG is labeled with a radioactive isotope ^{18}F (positron source), injected to patient, and accumulated in vulnerable plaques of coronary arteries. The radiation detector is then inserted into coronary artery, records positrons from FDG accumulated in vulnerable plaque, which allows for imaging and detection of the vulnerable plaque. A prototype detector was developed and tested. The detector consisted of a storage phosphor tip, light diffuser, optical fiber, and a thin plastic cover sheet. The detector is flexible, and has 2 mm diameter and 5 cm length. The detector was tested using realistic heart phantom with simulated vulnerable coronary artery plaques. The activities in simulated blood, heart tissue, and vulnerable plaques were matched to those expected in human anatomy. Since the storage phosphor detector is inserted into the coronary artery via x-ray fluoroscopy, the signal gathered from x-rays during the insertion process must be erased. Erasing was performed with a red laser light diffuser inserted into phosphor tip.

Results: The coronary artery plaques with 0.54 nCi mm^{-2} and 1.75 nCi mm^{-2} activities were reliably imaged with storage phosphor detector. The plaque with 0.18 nCi mm^{-2} activity was difficult to visualize over the noisy background. Literature reports that human vulnerable plaques are expected to have average area activities of 40 nCi mm^{-2}. Therefore, our detector can image plaques with activities by a factor of 20-70 lower than required.

Conclusion: The detector developed under this project can detect vulnerable plaques of human

coronary artery. However, the detector is a research prototype and currently is not suitable for *in-vivo* experiments. More efforts are needed to optimize its design for in-vivo applications.

CHAPTER 1 INTROUCTION

1.1 ATHEROSCLEROSIS

According to the World Health Organization, approximately one third of all deaths in developed countries are related to coronary artery disease [1]. Seventy percent of all myocardial infarctions are caused by soft plaque in the coronary artery which is vulnerable to rupture [2]. Burke defines artherosclerotic plaques as having a dense infiltrate of macrophages and, to a lesser extent, lymphocytes within a fibrous cap that overlies a crescentic, acellular mass of lipids (Figure 1) [3] [4]. Soft plaque is defined as a large confluence of fat, pushed out from the lumen by blood pressure and not yet organized with large amounts of fiber and cells. The risk factors such as inflammation, cytokines, bacterial and viral infections and homocysteine become significant in the endothelium (cap of the plaque) separating the plaques from the lumen of the coronary artery [2]. Recent research shows that sudden death caused by coronary disease is preceded by acute coronary thrombosis which is most frequently caused by plaque rupture [2]. Burke defines artherosclerotic plaques as having a dense infiltrate of macrophages and, to a lesser extent, lymphocytes within a fibrous cap that overlies a crescentic, acellular mass of lipids (Figure 1) [2] [3].

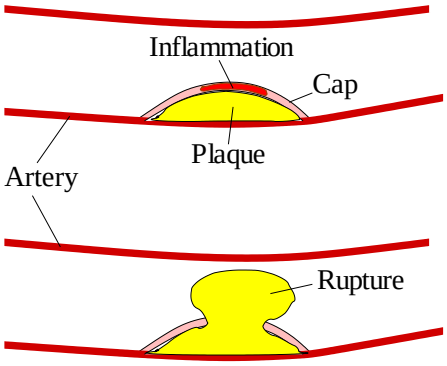

Figure 1. Artery plaque with inflamed endothelial layer (top). Rupture of endothelial level and detachment of plaque from the wall of the artery (bottom)

Atherogenesis begins at sites of endothelial injury [5]. Such injury may result from a variety of factors such as increased local shear forces from hypertension, elevated plasma concentrations of low density lipoprotein cholesterol and remnant lipoprotein particles, chemical toxins in cigarette smoke, low serum high density lipoprotein cholesterol and impaired reverse cholesterol transport, insulin resistance, and glycosylated end product formation [5]. As a result of these factors there is a decrease in endothelial cell production of nitric oxide, which impairs the protective functions of the vascular endothelium [5]. As a result of this, low density lipidprotein cholesterol is allowed to infiltrate the subendothelial space which after a series of cellular processes creates a site of inflammation [5]. Inflammation mediators infiltrate the developing lesion which triggers the development of a fibrous cap over the lesion [5]. The stability of advanced atherosclerotic lesion or plaque depends on its cellular and extracellular contents. Plaques with small lipid cores, thick fibrous caps, few inflammatory cells and a preponderance of smooth muscle cells are typically stable; conversely, those with large lipid cores, thick fibrous caps, numerous macrophages and relatively few smooth muscle cells are most likely to rupture [5] [6].

1.2 AUTORADIOGRAPHY

In the imaging technique of autoradiography, the radiation source to be imaged exists within the sample itself [7]. Biological processes can be studied by tagging a given substance with radioactive isotopes [8]. Although Fluorine-18is not a commonly used isotope for the purposes of autoradiography, due to its ready availability it was chosen for this project. If a thin layer of the sample is placed in contact with a radiographic emulsion over a sufficient exposure time, the beta particles emitted in the radioisotope decay will be recorded as an image on the developed emulsion.

Using these techniques, the detailed spatial distribution of radioisotope within the sample can easily be recorded [8].

1.3 FLUORODEOXYGLUCOSE

Activated leukocytes and macrophages have been reported to demonstrate increased 2-[fluorine-18] fluoro-2-deoxy-D-glucose (FDG) uptake in humans with different forms of infection [10]. Research performed by Sugawara indicates rapid accumulation of FDG in infectious foci and a high early target to background ratio. According to the Sokoloff [8] deoxyglucose method (Figure 2), which is analogous to FDG, deoxyglucose is transported by

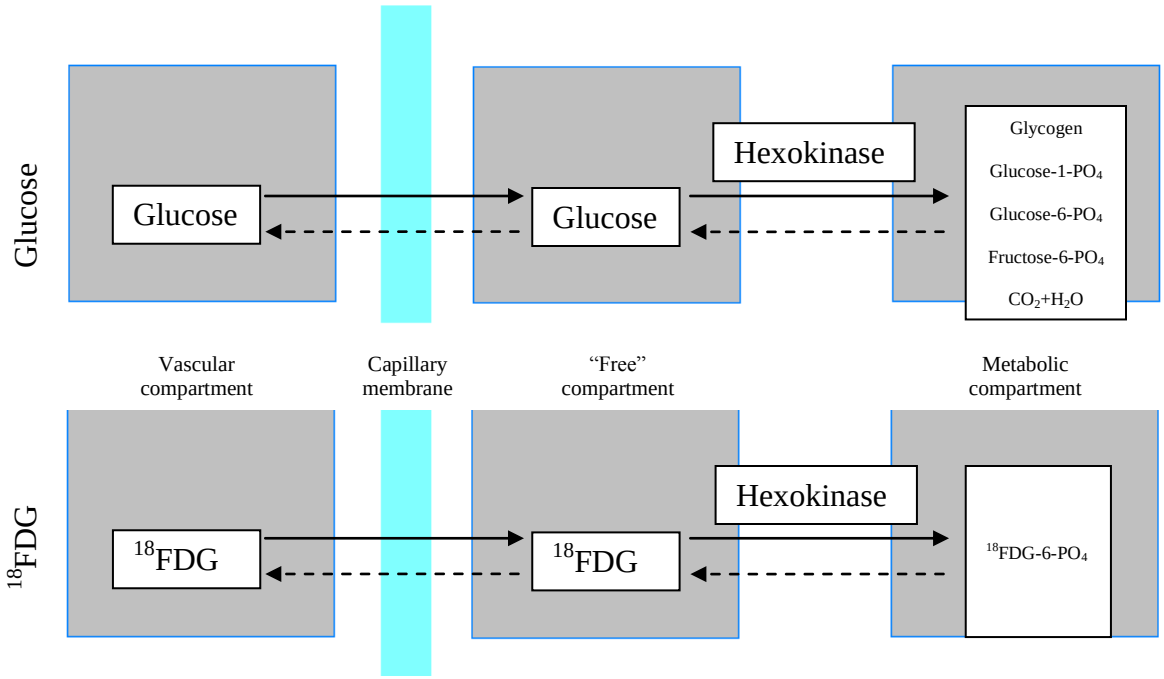

Figure 2. Transport and metabolic pathways for glucose and 2-deoxy-2[^{18}F]fluoro-D-glucose (FDG). Physically, the "free" compartment represents a combination of the interstitial space and the cytosol in both of which unphosphorylated glucose and FDG are uniformly distributed [8].

blood to the site of infection, where it is absorbed into the inflamed plaque by carrier-mediated diffusion mechanism. Hexokinase catalyzes the phosphorylation of glucose to glucose-6-PO_4 and FDG to FDG-6-PO_4. In both the transport and phosphorylation steps, FDG is a competitive

substrate with glucose [8]. FDG-6-PO_4; however is not a significant substrate for metabolism [8]. The conversion of FDG-6-PO_4 to glycogen is of low significance and it is not metabolized any further in the glycolytic pathway [8]. Since FDG-6-PO_4 does not diffuse across cell membranes, it gets trapped inside making it a useful imaging tool [8].

The activity concentration inside the blood after the injection of FDG into a patient was assumed to be 0.5 $x10^{-3}$ μCi mm^{-3}. This activity concentration was estimated for an injected activity of 15 mCi distributed in an average volume of a human of approximately 70 L; A slightly higher concentration is expected in active tissues such as the myocardium compared to bone for instance.

1.4 MORPHOLOGICAL IMAGING OF INTRAVASCULAR PLAQUES

Current methods of morphological imaging of coronary artery plaques include angiography, intravascular ultrasound, and intravascular MRI. These methods provide morphological information about structures of the inside of the coronary artery. They allow detecting plaques and determining its shape but do not allow determining inflammation status of the plaque.

1.4.1 Angiography

Angiography utilizes a radio opaque dye (typically iodine) which absorbs x-rays upon imaging using radiographic film[8]. The dye is injected into the coronary artery through a catheter which is inserted fluoroscopically from a main superficial artery (Figure 3). Before the contrast agent is injected to the artery a digital radiographic image of the patient's anatomy is taken. During and after injection a sequence of images is acquired. The image taken before the injection is then subtracted from the rest of the image. After the background subtraction the

silhouette of the coronary artery can be manipulated to provide morphological information about the shape and size of the coronary artery (Figure 3). This is temporal subtraction angiography[8].

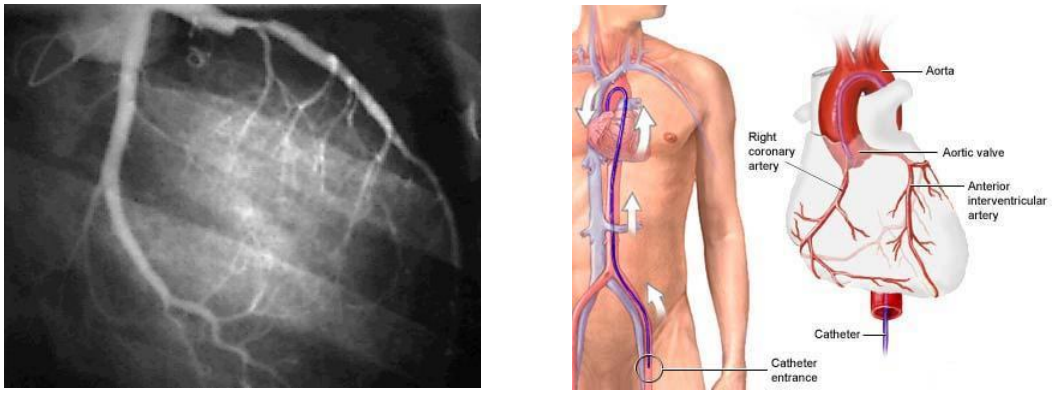

Figure 3. Coronary angiography catheter insertion through the femoral artery. Source www.nmh.org, www.harvard.edu

1.4.2 Intravascular Ultrasound

The use of intravascular ultrasound (Figure 4) for the imaging of plaque in the coronary artery was studied extensively by Tobis et al. [10]. Their preliminary study demonstrates the

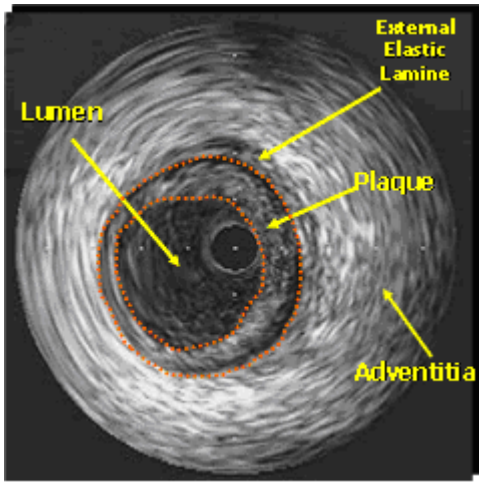

Figure 4. Intravascular ultrasound image. Orange line delineates plaque from the lumen. Source: www.incore.br

capability of intravascular ultrasound for providing real time cross sectional images of the coronary arterial lumen and wall in vivo. The ultrasound device consisted of a 1.2 mm

diameter cable with a 20 MHz transducer on the distal end with a mirror at 45º that reflects the beam perpendicular to the catheter [11]. The catheter was rotated by a motor at 1800 rpm to produce real-time cross-sectional images at 30 times sec^{-1} [11]. The imaging device was capable of providing information for the calculation of lumen geometry and the atheroma plaque cross sectional area. They also report on the ability to distinguish certain characteristics such as fibrous tissue, calcification, and lipid or necrotic within the atheroma plaque. They conclude that in comparison with angiography, intravascular ultrasound provides more detail about the morphology of the plaque[11].

1.4.3 Intravascular Magnetic Resonance Imaging

Intravascular magnetic resonance imaging (IVMRI) makes it possible to image coronary arteries in patients with ischemic heart disease, thus providing prognostic information that may be of more value than merely the number of lesions and degree of luminal obstruction, as currently detected by angiography [12]. IVMRI provides information about the thickness of the fibrous cap and the lipid core size which are important factors in determining plaque vulnerability. IVMRI may also be able to recognize and characterize plaque alterations such as intraplaque calcification and hemorrhage which may indicate the status of atherosclerotic plaque evolution. The intravascular ultrasound assembly consists of an external MRI scanner, and a receiver catheter coil inserted into the artery. Although, IVMRI provides information about the morphology (Figure 5) and to some extent composition of the plaque, it does not provide information about the inflammation status, which is of highest importance when determining the risk of thrombosis. IVMRI is more precise than x-ray angiography in quantifying atherosclerotic plaque size but is limited in the evaluation of plaque composition because of poor contrast resolution between different intraplaque components [12] [13].

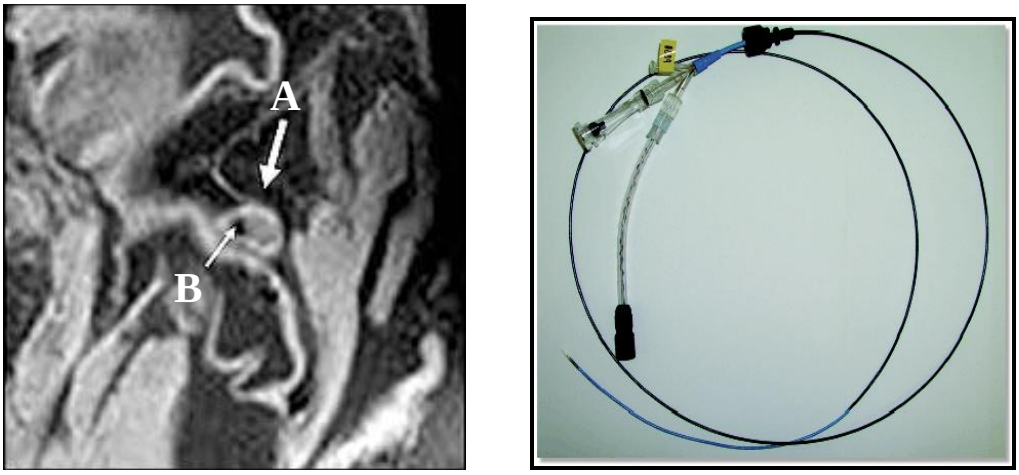

Figure 5. IV MRI of coronary artery plaque (left). A-coronary artery plaque. B-luminal narrowing. IV MRI instrumentation (right). Source: www.imagingeconomics.com, www.medgadget.com

1.5 FUNCTIONAL IMAGING OF INTRAVASCULAR PLAQUES

Although morphological imaging techniques can confirm the existence of plaque/blockage in the artery, they cannot determine the inflammation status of the soft plaque,

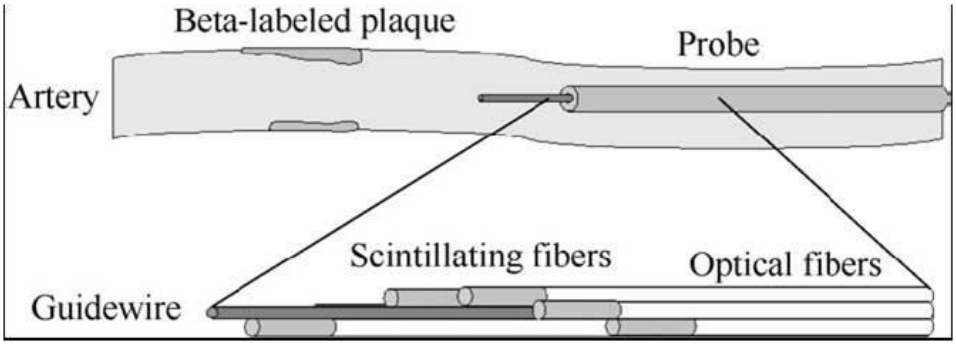

Figure 6. Miniature scintillation detector tip. Source: Rudd

which is of highest importance when assessing the risk of infarction [2]. This problem can potentially be solved using functional imaging methods. A radiotracer such as ^{18}F-fluorodeoxyglucose (FDG) is accumulated in the vulnerable plaques due to higher metabolic activity of the inflamed cap. The uptake ratio of the plaque versus soft tissue has been

determined to be based on animal studies to be 5.7 [10]. Since ^{18}F is a positron emitter with an approximate maximum positron range of 2.3 mm, the increased positron signal is detectable by a particle detector inserted directly adjacent to the coronary artery wall [7]. ^{18}F fluorodeoxyglucose is a suitable radiotracer for this purpose, readily available for clinical applications.

A catheter with a miniature positron detector has to be fluoroscopically inserted into the coronary artery, which requires the detector to account for or erase the signal acquired during the insertion process.

1.5.1 Positron Emission Tomography

Positron emission tomography (PET), has been studied as a modality for noninvasive imaging of arterial plaque by Rudd et al. [14] Their work demonstrated the ability to localize atherosclerotic plaque in the carotid artery with PET fused with a computed tomography image. In areas of high metabolic activity such as the heart and the brain, however, due to the small size of arterial plaque and low uptake PET is not suitable for the localization of coronary artery plaque [14]. Patient motion also presents a major obstacle when using PET as a modality for vulnerable plaque imaging.

1.5.2 Scintillation

Direct detection of positrons in the artery is possible using optical fibers with miniature scintillator tips in the end. This detector includes multiple optical fibers bunched together with scintillator tips in the end. Scintillators (Figure 6) are shifted relative to each other to increase the field of view of the detector. Although this detector system seems to be promising there are

multiple drawbacks associated with it. This detector has a limited number of pixels, limited field of view and low spatial resolution and sensitivity[15] [16].

1.5.3 Semiconductor Pixel Detector

A prototype of a device for beta imaging in the coronary arteries is being developed that uses a set of silicon detectors in series (Figure 7) [16]. The detector pixels are connected to each other via resistors, and each end of the pixel chain is readout with a preamplifier. The system uses a simple resistor network to divide the signal to allow differentiation of the location of the detector element of interaction by measuring the ratio of the signal at each end of the device. The major disadvantage of the silicon semiconductor pixel assembly is its size, which is too large for insertion into coronary artery when all necessary electronics are included.[16]

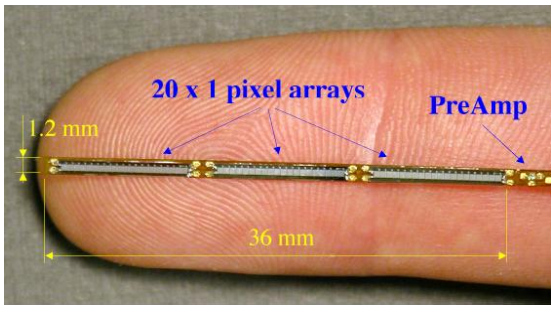

Figure 7. Photograph of PC-board with three 20 x 1 pixel array detectors coupled in series. A preamplifier is visible on the right end of the detector array

1.5.4 Storage Phosphor Positron Detector (Current Project)

The storage phosphor positron detector is based on a flexible tip made from a storage phosphor material. The diameter of the tip is chosen in the coronary artery. The length of the tip can also be matched to the vessel with no limitation [7]. The phosphor tip is bound to the end of a catheter used for an intravascular procedure. An optical fiber with a light diffuser at its end is incorporated into the storage phosphor tip. The light diffuser is used to erase the energy accumulated in the phosphor prior to exposure to positrons [7]. After FDG accumulates in the

vulnerable plaques, the phosphor tip is inserted into the artery. The positrons from the absorbed FDG are detected in various locations of the storage phosphor detector tip. After exposure the storage phosphor tip is removed and read out. The potential advantages of the storage phosphor positron detector are high spatial resolution and superior sensitivity to the positrons [7].

1.6 DETECTABILITY CRITERIA

According to the Rose model [17] visibility of low contrast elements in the image depends on object contrast, image noise, and size of the contrast element. The higher the object contrast, the lower the image noise, and the larger the contrast area, the higher the probability of detecting the contrast element [18]. A method commonly utilized for determining the effectiveness of imaging devices is contrast detail analysis. It represents a qualitative way of combining spatial resolution and contrast resolution. Using this technique an image is taken of a contrast detail phantom which contains increasing objects in rows with decreasing contrast in columns. The detectability of the objects is then plotted with the x-axis representing the size of the object and the y axis representing the contrast (Figure 8). After image acquisition a curve is drawn beyond which in the positive x direction objects can be distinguished from the background and in the negative x direction they blend in with the background. The curves on a contrast detail diagram indicate the transition from objects that can be seen to those that can not and these curves are derived subjectively by simple inspection. Although there is a level of interobserver variability, the contrast detail evaluation method works well as a qualitative assessment [9].

We have used a modified version of the contrast detail analysis when the size of the contrast element was fixed at 6.5 x 6.5 mm^2 and activity concentration was changed in the range of (0.12×10^{-3} $\mu Ci\ mm^{-3}$ - 36×10^{-3} $\mu Ci\ mm^{-3}$). The reason for not changing the size of the contrast element was limited information available about sizes and shapes of the vulnerable

coronary plaques. Postmortem autopsy studies have shown that the vulnerable coronary plaques may have complicated shape and may extend up to 20-30 mm along the coronary artery [15].

Also, it was technically difficult to produce simulated plaques with sizes significantly smaller than 6.5 mm x6.5 mm. Therefore, we have chosen the above size of the contrast element to perform initial analysis of the low contrast detectability.

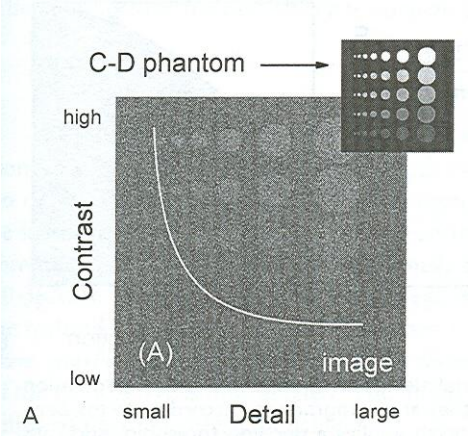

Figure 8. Contrast-Detail curve

1.7 STORAGE PHOSPHOR DETECTORS

1.7.1 Photostimulable Phosphor

The reason for doping the BaFBr with europium is that it creates defects in the BaFBr crystals which allows for electrons to be trapped more effectively. When the energy from ionizing radiation is absorbed by the phosphor crystals, it excites the electrons associated with the europium atoms [9]. This causes divalent europium atoms $<Eu^{2+}>$ to be oxidized and changed into trivalent $<Eu^{3+}>$ [9]. Excitation of the electrons allows them to become mobile and a certain portion of them gets trapped in F-centers. The trapped electrons remain in a higher energy metastable state for extended periods of time with a certain amount of fading [9]. The latent image before readout is composed of billions of electrons trapped in F-centers, with a

concentration proportional to the amount of x-ray exposure [9]. During the readout process of photostimulated phosphors low energy laser light interacts with the F-centers and transfers energy to the electron. The electron is given enough energy to reach the conduction band, which enables it to be mobile again. Many electrons get reabsorbed by the trivalent europium atoms while emitting blue and green light [9]. This light is then recorded by the photomultiplier tube and subsequently turned into a digitized signal[9] [19].

1.7.2 Interaction of Positrons with Storage Phosphor Plates

Storage phosphor materials are sensitive to positrons making them suitable for the fabrication of storage phosphor detector tips for determining the inflammation status of vulnerable coronary artery plaque based on increased positron emission. There are four factors that determine the sensitivity of the storage phosphor detector tip: (1) fraction of positrons that have an initial direction toward the phosphor tip; (2) fraction of positrons that are absorbed in the blood surrounding the phosphor tip; (3) energy loss of positrons in the blood; and (4) stopping power of the phosphor for positrons [7]. The positrons are emitted from the plaque with isotropic angular distribution and a fraction of them has an initial direction towards the phosphor tip. This fraction is called geometric efficiency and it was determined by the geometry, which is the diameter of the phosphor tip and the gap between the phosphor tip and the plaque. A fraction of the positrons is absorbed in the blood layer between the phosphor tip and the surface of the plaque. While traveling in blood the average energy of the positrons is decreased according to the exponential relationship between the positron transmission through material and the material thickness [20-21]. Also some of the positrons entering the phosphor are not absorbed due to its limited thickness. Absorption efficiency of the phosphor layer with a known thickness was calculated using the chemical composition and average density of the phosphor layer.

Linear stopping power for charged particles in a given absorber is defined as the differential energy loss of that particle within the material, divided by the corresponding differential path length. The stopping power for positrons in blood with respect to the energy of the positrons is plotted in Figure 9.

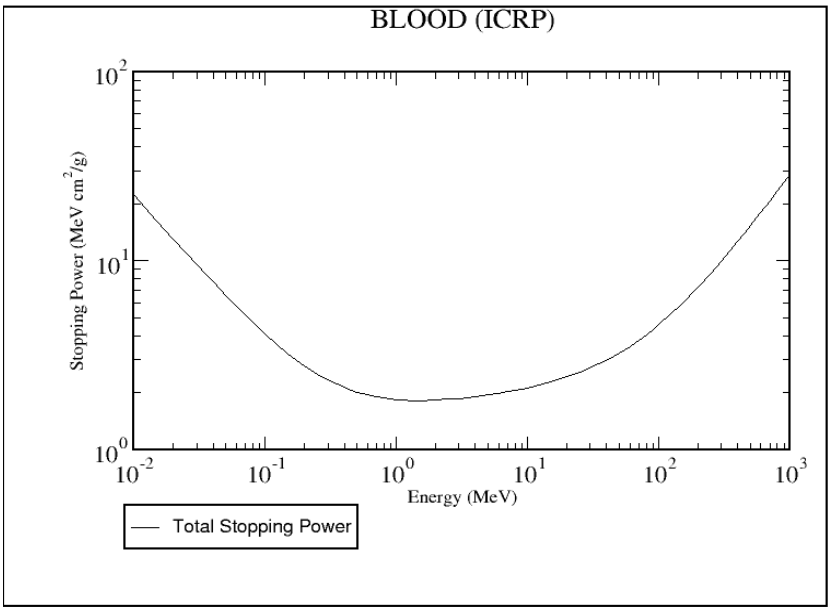

Figure 9. Total stopping power of blood for positrons with respect to energy. Blood density is defined according to ICRP. Source NIST

For ideal imaging conditions the distance between the storage phosphor detector and the coronary plaque would be minimal. However, since the detector is inserted inside the coronary artery, blood flow can only be obstructed to a certain limit. Depending on the diameter of the artery the relationship between blocked fraction as a function of gap thickness was plotted in Figure 10. The ideal compromise between obstruction and functionality is a gap thickness of 0.6 mm. The average positron range in blood for FDG is 0.6 mm, therefore if the gap is larger most of the positrons will get absorbed in the blood instead of being detected by the storage phosphor detector tip.

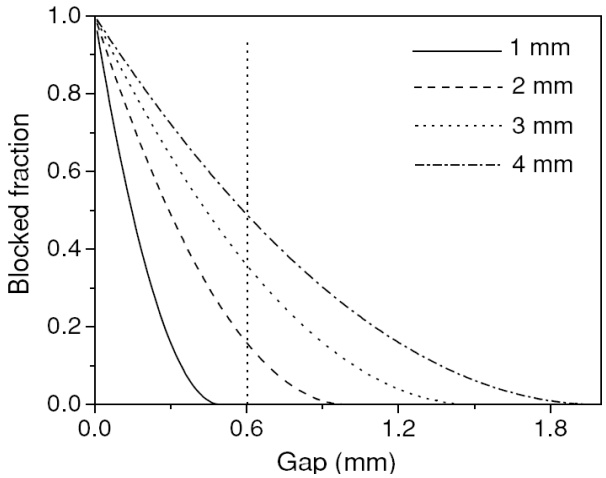

Figure 10. Fraction of the artery cross section blocked by storage phosphor tip vs. gap between phosphor tip and artery wall, for 1 mm, 2 mm, 3 mm and 4 mm diameter arteries. Vertical marker drawn at 0.6 mm, which is the average range of the ^{18}F positrons in blood. It is preferable to keep the gap between tip and artery wall less than 0.6 mm, otherwise most of the positrons emitted from the plaques will be absorbed in the blood and will not reach the phosphor tip. [7]

1.8 PURPOSE

The purpose of this study was to develop and investigate an intravascular storage phosphor detector for the imaging of the accumulation of fluorodeoxyglucose (FDG) in vulnerable coronary artery plaques with inflammation of the endothelial cap. The concept of the intravascular detector was originally proposed in [7] This project was supported by an NIH grant R21EB006142-01(Dr. Shikhaliev PI). The material included in this thesis was generated based on the research concepts described in preliminary study and research design parts of the above NIH grant.

1.9 HYPOTHESES AND SPECIFIC AIMS

The hypothesis of this work is that intravascular autoradiography detector based on storage phosphor can detect an FDG uptake of 40 nCi mm^{-2}. This uptake is typical to that accumulated

in vulnerable plaques of the human coronary artery. Five aims have been completed to test this hypothesis.

Aim 1. Storage Phosphor Tip Fabrication. Fabricate storage phosphor tip from photostimulable phosphor material to meet the dimensional requirements of the coronary artery without causing a lethal obstruction for blood flow.

Aim 2. Detectable Activity Concentrations. Determine the detectable range of activity concentrations of FDG using storage phosphor plates of same material as intravascular storage phosphor detector tip. Use commercially available Kodak storage phosphor plate with high-sensitivity and low resolution, to measure the difference in signal deposited at different activity concentrations. This is to be performed using a wide range of activity concentrations, which also should include activities comparable to those expected in the coronary artery plaques.

Aim 3. Erasing efficiency of the storage phosphor system. (using white light, red laser light, patient phantom) Determine the amount of signal erased by white light and red light after irradiating the storage phosphor tip for a duration of time equal to that of the fluoroscopic insertion. Determine the minimum amount of residual signal which cannot be further erased from the storage phosphor tip. Consequently quantify the amount of background signal coming from different sources.

Aim 4. Testing of storage phosphor detector in patient like using heart phantom. Build a realistic heart phantom from tissue equivalent material that includes myocardium with typical clinical activity concentration of FDG, coronary arteries with realistic diameters and filled by blood equivalent material at a typical FDG concentration, and coronary artery plaques with expected amount of FDG uptake.

Aim 5. Scattered Gamma Signal. Determine the impact of scattered gamma photons from heart

tissue on the beta signal collected from coronary artery plaque. Quantify the fraction of deposited signal from the positron source, compared to the scattered photon background. Determine minimum activity in the plaque that can be detected over the scattered gamma background.

CHAPTER 2 METHODS AND MATERIALS

2.1 AIM 1: STORAGE PHOSPHOR TIP FABRICATION

The detection of positron signal from vulnerable plaques inside the coronary artery requires a detector which can be fluoroscopically guided via catheterization into the coronary artery and gather signal without creating a lethal obstruction inside the blood vessel. Since the catheter with the miniature positron detector must be fluoroscopically inserted into the coronary artery, this requires the detector to account for or erase the signal acquired during the insertion process. The compositional characteristics of storage phosphor materials are suitable for the fabrication of a detector that can be erased with an intense light source inside the coronary artery, restoring the original imaging ability of the detector. The storage phosphor material, commonly shaped as large flat plates for imaging, can be formed into miniature hollow cylinders mimicking the length of the coronary artery with space for a thin, high-intensity laser light diffuser.

A prototype storage phosphor tip was fabricated using a commercial medium density, high sensitivity, low resolution storage phosphor plate. High sensitivity of the plate is necessary because positron signal from plaques are anticipated to be very low [7]. For storage phosphor plates there is a tradeoff between sensitivity and spatial resolution. High sensitivity plates provide low resolution, and vice versa. However, high resolution of typically 0.1-0.2 mm is not required for imaging vulnerable plaque. Such a high resolution would require high counting statistics either from large activities or long counting times to achieve acceptable signal to noise ratio for reliable detectability. This level of signal statistics cannot be provided with the small activities accumulated in vulnerable plaques. The thickness of the phosphor plate was 0.81 mm which included a 0.25 mm thick layer of BaFBr, a 0.4 mm thick flexible support layer and a 0.16

mm thick light reflector incorporated between the BaFBr and support layers. A thin 6.5 cm by 0.45 cm strip was cut out from the original storage phosphor plate. The top phosphor layer was gently separated from the thick flexible support layer. This was performed by gripping the edge of the flexible support layer and slowly bending it until the phosphor layer became completely detached (Figure 11).

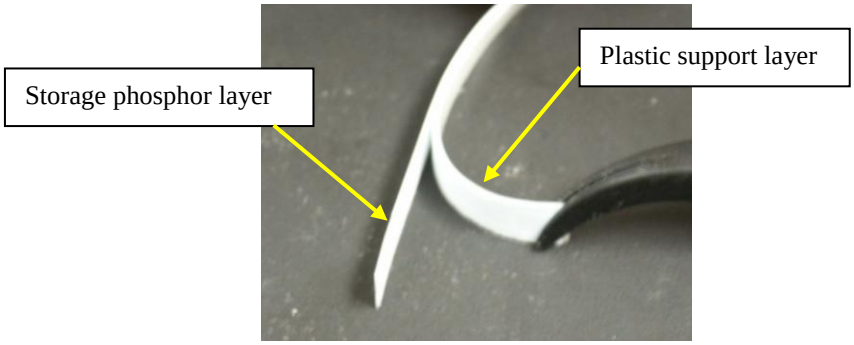

Figure 11. Separation of storage phosphor layer from flexible support layer.

The resulting thin layer of storage phosphor material was very fragile so it was pressed onto the adhesive layer of clear plastic tape, the surface area of which was cut to match the area of the phosphor layer. Although the experiments throughout this research used the plastic tape as backing, a thin layer of epoxy was reported to be more adequate for increased elasticity of the storage phosphor tip [7]. Using tape however, was more reliable and reproducible for our experiments. The thickness of the tape was less than 0.05 mm. Care was taken while applying the phosphor strip to the tape to ensure that the side of the phosphor with the clear emulsion was facing away from the adhesive layer of the clear plastic tape. This was ensured by marking the layer of the storage phosphor substrate which contained the emulsion with a small dot prior to separation from the plastic base layer.

The storage phosphor material too fragile to roll into a small diameter cylinder. Therefore, the storage phosphor tip was fabricated using a segmented configuration of the

phosphor tube, where the small segments of phosphor material were assembled over the clear flexible adhesive base (Figure 12).

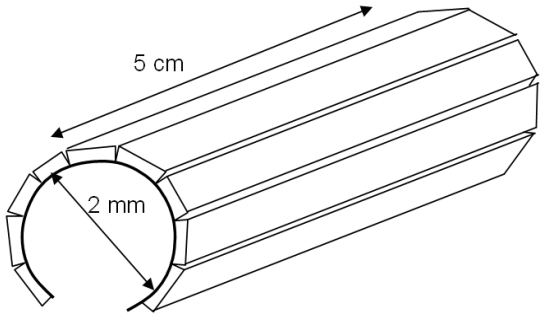

Figure 12. Schematic of ideal storage phosphor detector tip with multiple segments.

Segmentation was achieved by using a razor blade to cut fine groves into the phosphor layer of a larger strip. Care was taken not to cut completely through the clear plastic tape. The razor blade was placed directly perpendicular to the narrow side of the strip and parallel to its long side. By exerting uniform pressure on the razorblade, the storage phosphor layer split down to the clear plastic tape (Figure 13). The exertion of pressure was halted immediately after the storage phosphor layer had been cut.

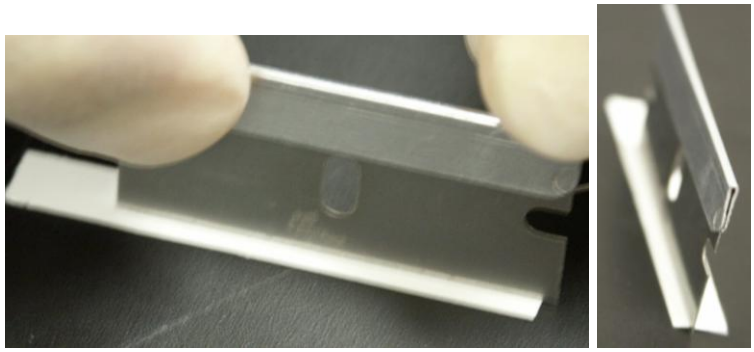

Figure 13. Cutting longitudinal segments into storage phosphor material using a razor blade.

Because the phosphor was fragile there was a limitation as far as the number of cuts that could be performed before the storage phosphor material became unstable. With too many cuts,

the individual segments began to crumble and to detach from the adhesive tape layer. In our experiment four segments represented the ideal compromise between functionality and rigidity (Figure 14, 15). The arrangement of the four segments created a rectangular cross section instead of a cylindrical one.

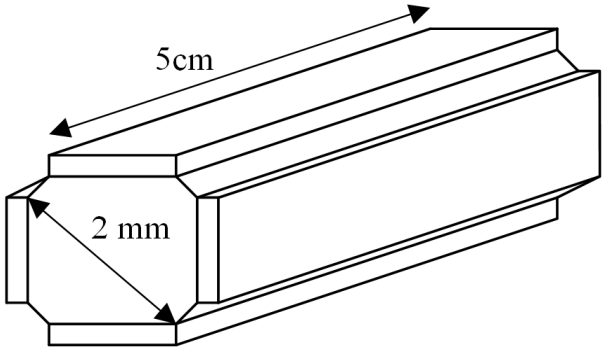

Figure 14. Schematic of storage phosphor tip used in experiments.

The width of the individual segments varied somewhat, were approximately 1.4 mm. The variation in the width of the individual storage phosphor segments was attributed to the lack of more precise cutting and measuring equipment. This 4-segment design put a limitation on the field of view and decreased the spatial sensitivity of the storage phosphor detector tip due to the gaps.

Figure 15. Flattened storage phosphor detector tip with four segments.

Once the storage phosphor was segmented, the cylinder was inserted inside a sturdy clear plastic tube. The tube had an inner diameter of 2 mm, with a thickness of 0.01 mm and a

length of 8.4 cm. The loose edges of the storage phosphor tip were not physically attached to each other; the tube held the storage phosphor tip in the cylindrical shape. The inner diameter of the storage phosphor tip inserted inside the clear plastic tube allowed enough clearance for the insertion of a laser light diffuser attached to the distal end of a thin fiber optic cable.

2.2 AIM 2: DETERMINE THE MINIMUM DETECTABLE ACTIVITY CONCENTRATION OF ^{18}F

Currently there is no experimental data available on uptake ratio of FDG in vulnerable plaques of the human coronary artery. The uptake ratio of FDG inside rabbit coronary artery plaque relative to the concentration of FDG within the bloodstream was determined to be approximately 5.7 based on post mortem studies [15]. It is reasonable to assume that the uptake of FDG inside vulnerable plaque of the human coronary artery would demonstrate a similar increase. Using the value of 5.7 predicts that vulnerable plaque may have a potentially high probability of detection with a miniature positron detector placed adjacent to the internal wall of the coronary artery. To determine the minimum detectable activity concentration that the detector can distinguish from background, a series of experiments was devised.

To simulate the uptake of FDG within vulnerable plaque inside the coronary artery a material had to be identified which would imitate the characteristics of the vulnerable plaque filled with FDG. A thin sheet of porous silica material of a total thickness of 0.38 mm on a plastic base was chosen as the ideal material for this experiment [7]. Porous silica is SiO_2 the FDG solution and distribute it evenly throughout the entire volume of the porous silica material. This quality of the material was important for achieving homogenous distributions of FDG solution in porous silica squares of various volume.

Multiple squares with the dimensions of 6.5 x 6.5 mm^2 were cut out of a large sheet of porous silica material. The porous silica layer was then separated from the plastic base

layer using double sided, clear, adhesive tape (Figure 16). The reason for removing the prous silica layer was the rigidity of the base layer which would make it impossible for the porous silica material to be wrapped around the coronary artery phantom. Because the adhesive material on the double sided tape proved to be stronger than the adhesion of the silica to the plastic base, the porous silica was easy to remove from the base by attaching one side of the double sided tape to the top layer of porous silica.

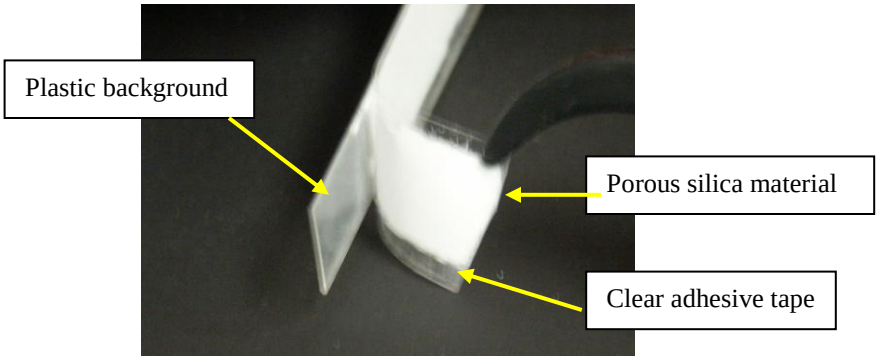

Figure 16. preparation of porous silica layer from flexible plastic background.

A thin acrylic plate was fabricated that would serve as a base for the porous silica squares to be filled laterwith FDG solution (Figure 17). An outline of the shape of a standard storage phosphor plate was drawn on the top of the acrylic plate. The dimensions of this outline were 25.0 cm and 12.5 cm. Within the boundaries of the storage phosphor plate outline, nine squares were drawn of 6.5 x 6.5 mm dimensions in three rows and three columns at uniform distances. The porous silica squares were positioned on the squares marked on the acrylic plate with the adhesive side facing the plate.

^{18}F-FDG (Cardinal Health Baton Rouge, LA) was diluted to specified activity concentrations to create a scale of activity concentrations for our measurements. The target scale for our measurements ranged from 0 μCi mm^{-3} to 40 x10^{-3} μCi mm^{-3}. FDG solution was

delivered in a syringe inside a shielded magazine. Appropriate protective clothing was worn at all times during the series of experiments to prevent any contamination of the skin.

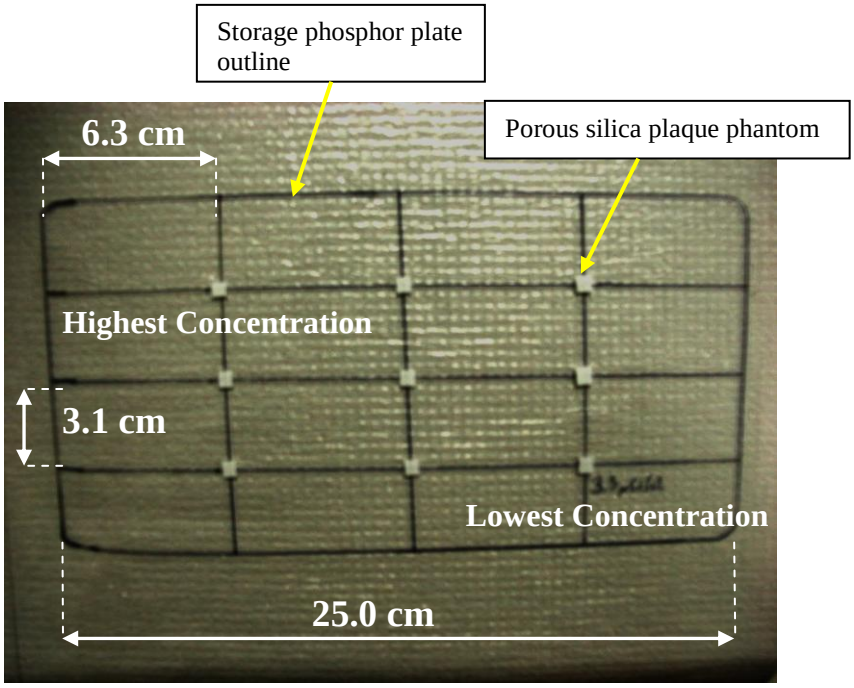

Figure 17. Grid layout of porous silica squares on thin sheet of acrylic.

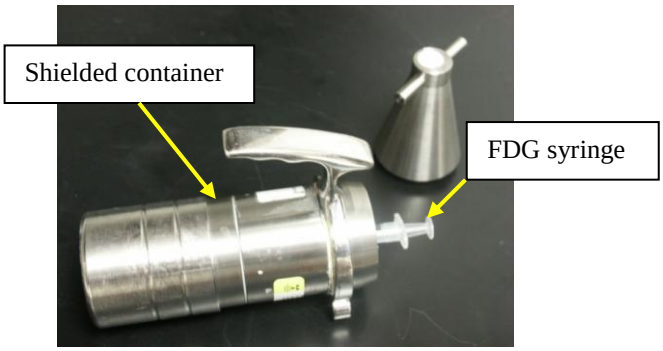

Figure 18. Shielded container with FDG syringe.

Immediately after delivery, the syringe from the shielded container (Figure 18) was placed in an Atomlab 100 (Biodex Medical Systems) dose calibrator chamber (Figure 19) to record the initial activity concentration of FDG within the syringe. The error associated with

dose calibrator measurements was +/- 0.5 µCi for activities greater than 100 µCi; error of +/- 0.05 µCi or +/- 10% (whichever is larger) for activities less than 100 µCi.

A small amount of the initial solution was then transferred into a smaller 10 mL syringe and the activity concentration inside of the 10 mL syringe was quantified via the dose calibrator. The volume error associated with the 10 mL syringe was +/- 0.05 mL. Based on the reading was to, the FDG solution inside the small syringe was diluted with water to achieve the desired

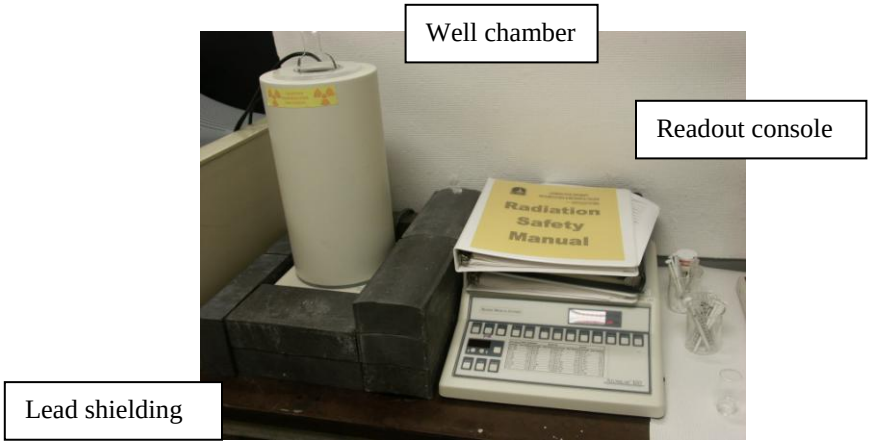

Figure 19. Biodex Medical Systems – Atomlab 100 dose calibrator (well type chamber)

activity concentration (Figure 20). This process was repeated for each desired activity concentration, while recording the time of dilution and marking each syringe according to the activity concentration contained within. The activity at the time of dilution was scaled up from the desired activity for the experiments to account for radioactive decay. The recorded times were used after each experiment to calculate exact activity concentrations at the time of the experiment. Equation 1 was used to calculate the activity in all experiments regarding exponential decay.

$$A = A_0 * e^{\frac{\ln(2)*t}{t_{\frac{1}{2}}}}$$

Equation 1. Time dependent exponential decay

A_0 = initial activity of FDG

A = activity at the time of measurement

t = duration of time between activity calibration and signal measurement

$t_{1/2}$ = half life of ^{18}F (109.77 min)

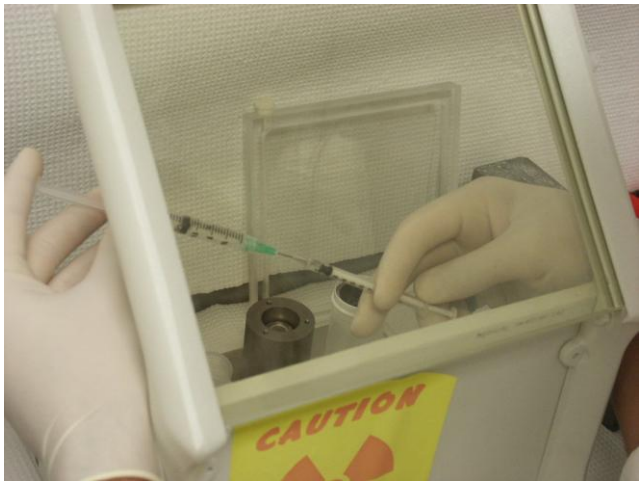

Figure 20. Dilution of high concentration FDG.

The porous silica squares previously attached to the acrylic plate were filled with the FDG solutions in an increasing order. The nine porous silica squares were each labeled for an activity concentration corresponding to those contained in the syringes. Each FDG solution was transferred from the 10 mL syringe into a small plastic cup. From each cup, a pipette was used to draw up the solution and to deposit a 10 µL volume onto the porous silica square with a matching label (Figure 21). Using a pipette was necessary to accurately measure such small volumes of solution. The volume error for the pipette was +/- 0.1%.

The volume of deposited FDG solution corresponded to the volume that can be absorbed on a porous silica square with the dimensions of 6.5 x 6.5 x 0.25 mm^3. The process described above was repeated for each activity concentration. The squares were gently dried with a heat

gun (Alpha Wire Company MG-1 Heat gun 360 W) for approximately 3 minutes. The acrylic plate with the porous silica squares was transferred to a dark room where it was imaged with a

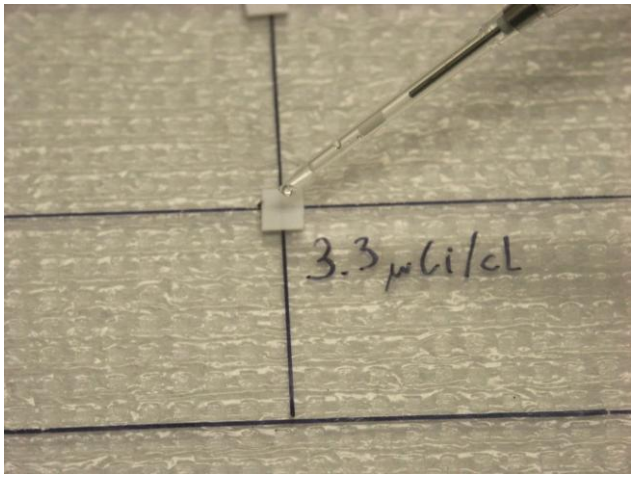

Figure 21. Deposition of diluted FDG onto porous silica square.

high sensitivity low resolution storage phosphor plate. The phosphor plate was previously erased by a 30 W Porta trace 1118 flat panel white light source for a standard erasing time of 10 minutes (Figure 22). Prior to each measurement the storage phosphor material was erased for a

Figure 22. The Porta trace 1118 flat panel white light source produces a 30 W flood of light, used for erasing storage phosphor plates.

period of 10 minutes, to eliminate residual signal from previous experiments and to maintain a consistent background noise level.

The detector was placed directly on top of the squares with the phosphor side of the plate facing towards the squares. The time of data acquisition was recorded. In complete darkness beta and scattered gamma signal was collected by the storage phosphor plate for two minutes. The 2 minute exposure time was chosen because this represents the time during which the intravascular detector can be located inside the coronary artery without becoming a lethal obstruction. The storage phosphor plate was transferred into a light tight envelope and the plate with FDG sources was moved away. The storage phosphor plate was then inserted in the Perkin Elmer Cyclone Storage Phosphor readout system (Figure 23) and the image was read out. For the readout procedure the lowest resolution setting was chosen (150 DPI).

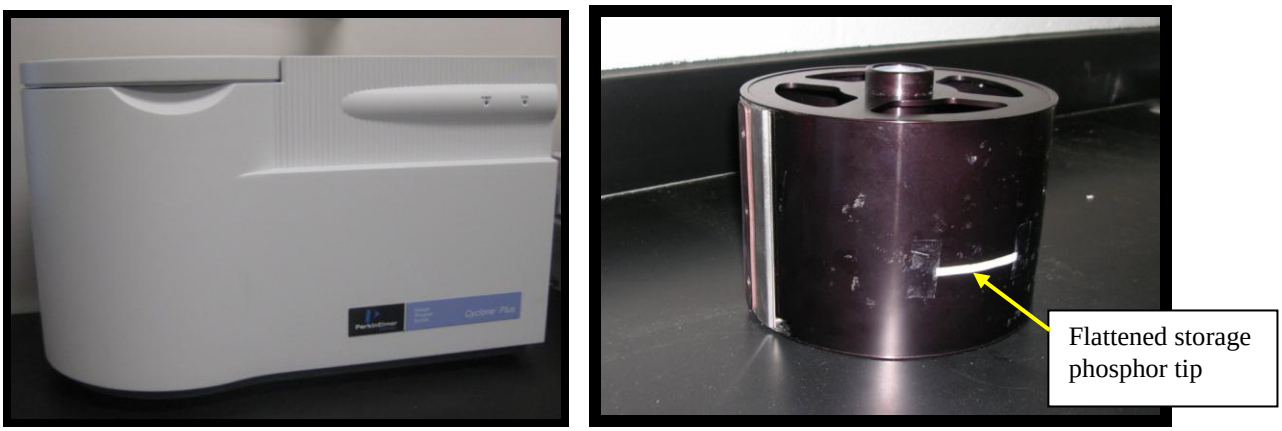

Figure 23. (Left) Perkin Elmer Cyclone storage phosphor readout system. (Right) Flattened Storage phosphor tip attached to drum of readout system.

The digitized images of the deposited signal were saved as TIFF files and processed using the ImageJ-NIH developed Java based image processing software. All acquired images were transformed from 16bit to 32 bit images. The pixel values within the images were squared in order to overcome the square root factor which was used to display images by the Cyclone software. After image processing decay correction calculations were performed for the individual activity concentrations based on the time interval that passed between dose calibration and data acquisition.

An alternative method for creating a scale of detectable activity concentrations utilized the natural decay of ^{18}F with a half life of 109.77 min [8]. This experiment was performed to bypass the physical process of dilution and compare the results of the two independent procedures in case the dilution process proved to be inaccurate. For the experiment four 6.5 x 6.5 mm^2 porous silica squares were attached to a clear acrylic sheet following the method of square deposition from the previous section. ^{18}F-FDG was assayed and the time of readout was recorded for decay corrections. For this experiment only two activity concentrations were used in comparison with the previous experiment which required nine dilutions. Part of the FDG solution was diluted with water to reach a target activity concentration of approximately 40 x 10^{-3} $\mu Ci\ mm^{-3}$. The remainder of the original solution was diluted with water to get an activity concentration of approximately 10 x10^{-3} $\mu Ci\ mm^{-3}$. The syringes were labeled according to the amount of activity contained within them. The two sets of two porous silica squares on the acrylic sheet were also labeled in correspondence with the amount of activity present inside the syringes. A volume of 10 mm^3 of the 40 x10^{-3} $\mu Ci\ mm^{-3}$ solution was deposited onto each of the first set of two porous silica squares, while the same volumes of 10 x10^{-3} $\mu Ci\ mm^{-3}$ solution were applied to the second set of two porous silica squares. Using the same activity concentration for two adjacent squares provided a duplicate data point for each activity concentration. After the deposition of solutions the acrylic sheet was taken to the dark room. A high sensitivity, low resolution Kodak storage phosphor plate was erased by white light source for 10 minutes. The plate was placed on the acrylic sheet with the phosphor side of the plate in contact with the porous silica squares. Immediately after the plate was positioned on top of the acrylic sheet the lights in the dark room were switched off and the data acquisition began. The time of data acquisition was recorded for decay corrections.

The plate remained on top of the acrylic sheet for an acquisition time of 2 minutes. The 2 minute exposure time was chosen because this represents the time during which the intravascular detector can be located inside the coronary artery without becoming a lethal obstruction. The plate was removed, placed inside of a light tight envelope, and removed from the proximity of the source to avoid contamination. The next set of measurements took place after the period of one half life ($t_{1/2}$ = 109.77 min). The plate was taken out of the light tight envelope and placed on top of the acrylic sheet, shifted in the longitudinal direction by 2 cm. The plate remained on top of the acrylic sheet for the same acquisition period of 2 minutes. The above process was repeated seven times, resulting in 14 different activity concentrations that appeared to be imaged side by side. At the end of data acquisition the storage phosphor plate was placed in a light tight envelope and the source was removed from the room. The storage phosphor plate was then removed from the envelope and inserted in the storage phosphor readout system. The plate was read out and the data was processed in the same manner as the previous experiment.

2.3 AIM 3: DETERMINE THE ERASING EFFICIENCY OF THE STORAGE PHOSPHOR SYSTEM

Placement of the storage phosphor tip into the coronary artery is achieved by attaching the tip to a guide wire and inserting it through the femoral artery to the coronary artery. Real time imaging of the location of the guide wire is necessary for the physician to be able to guide the catheter to the coronary artery. Real time imaging for this purpose is achieved by the method of fluoroscopy.

Fluoroscopy is an imaging procedure that allows real-time x-ray visualization of the patient with high temporal resolution commonly used for angiography. Most cardiology catheterization suites are equipped with an angiography system with the x-ray tube and image intensifier mounted on a C-arm configuration, which allows easy adjustments between the lateral

and poster anterior imaging positions. In most cardiology catheterization units a 23 cm image intensifier is used.

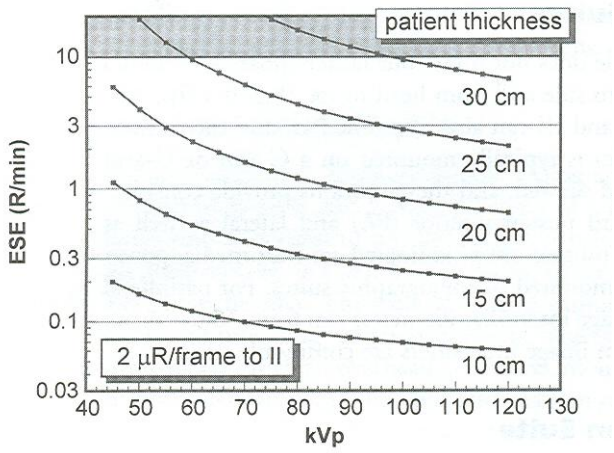

Figure 24. The entrance skin exposure is a function of kVp for different patient thicknesses. As the kVp increases, the entrance skin exposure at all patient thicknesses is reduced. Thick patients imaged at low kV suffer the highest entrance skin exposures. Entrance skin exposure values above 10 R/min are restricted by regulations (gray zone) and the fluoroscopic system has safeguards to prohibit these exposure rates. Source: Bushberg et al.

The total exposure delivered to the phosphor tip depends on the exposure rate and the duration of the fluoroscopic insertion process. The latter is estimated to be approximately 300 second [7]. The exposure rate can be estimated from Figure 24 which relates entrance skin exposure rate to x-ray voltage for various patient thicknesses.

Once the guide wire with the phosphor tip has reached the coronary artery, the storage phosphor tip must be irradiated by a bright light source to erase the fluoroscopic signal accumulated in the phosphor. Unlike the flat panel light source used to erase conventional storage phosphors, the phosphor tip requires the light to be delivered down the length of the catheter via an optical fiber. At the tip, a diffuser is needed to redirect the light through the phosphor cylinder.

To erase the signal accumulated in the storage phosphor tip during the fluoroscopy-guided insertion, the tip must be illuminated with bright light. For a conventional storage phosphor plate, this is achieved with a large area source such as the PortaTrace light described previously. For the storage phosphor tip, light must be piped from an external source via optical fiber through the catheter. A conventional light (e.g. incandescent or fluorescent) would be inefficient at coupling light into the optical fiber. A white emitting diode (LED) could be more easily coupled to the optical fiber, but may not produce adequate intensity. In both cases, these sources will be limited in their ability to deliver sufficient light to the storage phosphor were 10 J cm^{-2} is required to reduce any signal by a factor of 10^{-5} [7].

A third alternative is a laser diode. A laser diode can be coupled efficiently to the optical fiber and provides sufficient intensity to erase the phosphor. However, laser diodes that emit white light are not commonly available; red laser diodes are available, but the long red wavelength is expected to be less efficient at erasing than white light, which contains blue and green wavelengths. Described below, we evaluated the erasing efficiency of a red laser diode, comparing it to the large-area PortaTrace white light source.

An additional complication is that the erasing light, which becomes collimated longitudinally as it travels down the optical fiber, must be redirected radially to illuminate the cylindrical phosphor layer at the tip. A light diffuser, placed within the hollow phosphor cylinder at the end of the optical fiber, scatters the light to produce uniform illumination of the storage phosphor.

In this prototype, a red-laser diode with controller and a light diffuser were implemented. The length and outer diameter of the storage phosphor tip were approximately 5 cm and 2 mm respectively, which produces a surface area of 1.57 cm^2. An erasing exposure of requires 15.7 J of energy to be delivered by the light diffuser [7]. Applying a light exposure of 10 J cm^{-2} to the

storage phosphor tip results in the reduction of the signal to less than 10^{-5} of the original exposure level.

In this prototype, residual signal was removed using a red laser light and optical diffuser that is approximately 5 cm long matched to the length of the phosphor tip (Figure 25). The diameter of the light diffuser was 0.2 mm in diameter which fits inside the cylinder created by the phosphor tip.

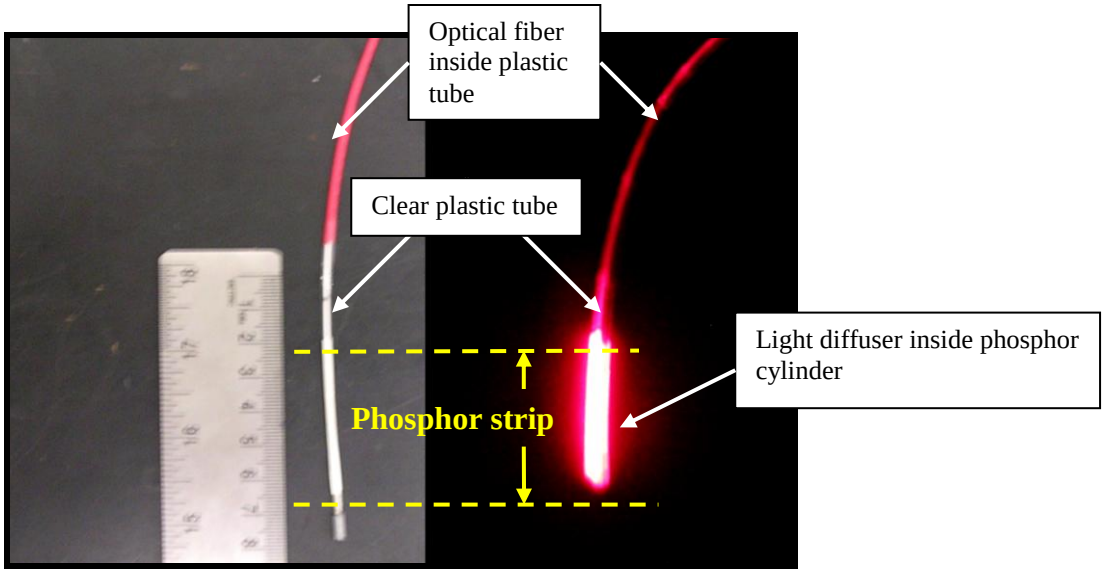

Figure 25. Laser light diffuser inserted inside of the storage phosphor tip. Image taken of identical setup with room lights on and laser light off (left) and with room lights off and laser light on (right).

To erase the signal accumulated in the storage phosphor detector during fluoroscopic guided insertion, a light source had to be chosen. Because a laser light diffuser must be inserted into the storage phosphor cylinder, the dimensions of the light diffuser must be small, yet powerful enough to erase the signal deposited on the detector via fluoroscopy to background.

2.3.1 Erasing Mechanism

The Combi-Z laser Diode Controller (Figure 26) consists of a stabilized laser diode driver, a temperature controller, and a laser diode connector. The driver allows continuous

adjustment of the output power over an operating range of 0-1000 mA. Laser diode temperature is controlled by a thermoelectric cooler with feedback from a thermistor that is typically incorporated in 14 pin butterfly packages.

The Combi-Z laser Diode Controller was attached to a single stripe laser diode mounted in high heat load (HHL). The HHL laser diode series is a high power (350 mW-3.0 W) diode laser mounted in a high heat load package, which operates in continuous wave mode. The

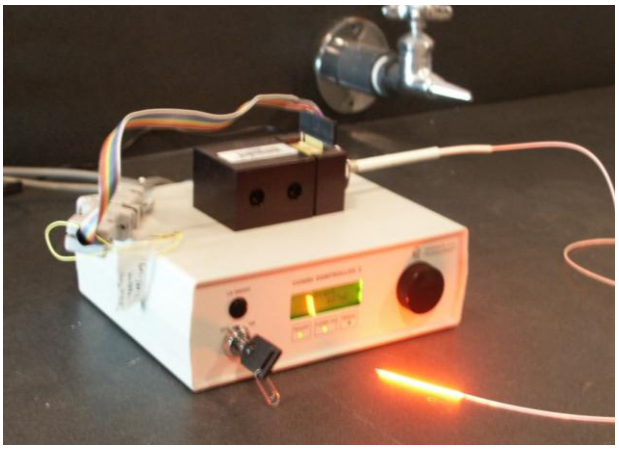

Figure 26. Combi-Z laser Diode Controller connected to Single Stripe Laser Diode Mounted in High Heat Load

precise wavelength and optical power are a function of the laser diode temperature and operating current. The diode begins to lase when the drive current exceeds the threshold current. Further increase in current causes a linear increase in optical power up to a specified maximum operating power.

External to the catheter, the erasing light was collected from a light source using a reflector and focused into the optical fiber. White light erases the phosphor plate with higher efficiency compared to red light due to the shorter blue and green wavelengths present in the white light. However, the laser is more efficient at transferring light into the optical fiber to the small surface of the storage phosphor detector, so that the detector receives a higher intensity of the red light compared to the unfocused white light.

To select the best light source, an experiment was devised comparing the erasing efficiency of white light to red laser light. However, the intensity of the two sources was not identical and the method of exposing the phosphor tip to the light source also varied between the two sources. The goal of this comparison was to generate a graph which at long periods of erasing would quantify the erasing efficiency of the two light sources. Two storage phosphor tips were exposed to white light source (Porta Trace 1118 flat panel light source) for 10 minutes to reduce any previously acquired signal to background level. The tips were then enclosed in a black light tight envelope on a thin cardboard base. The envelope was placed in the radiation field of an OEC Diasonics 9000 C-arm fluoroscopy X-ray unit at the level of the image intensifier (Figure 27).

The machine was set at a current of 0.5 mA and a voltage of 70 kVp. The phosphor tip was irradiated to near saturation of the readout device which was approximately at an arbitrary signal level of 60,000 A.U. This was the largest signal level which could be reproduced readily on the phosphor plate without oversaturating the readout device, which occurred at a signal level exceeding 64,000 A.U. Reaching this signal level was controlled by keeping the duration of exposure constant and monitoring the entrance dose by an ion chamber.

Once this level was reached, the light tight envelope was transferred to a dark room; the room had to be kept dark because exposure of the storage phosphor tips to any light other thanthat used in the erasing experiment would have erased a portion of the deposited signal. The phosphor tip to be erased by red light was removed from the envelope and inserted in the clear plastic tube in order for the tip to take on a cylindrical shape.

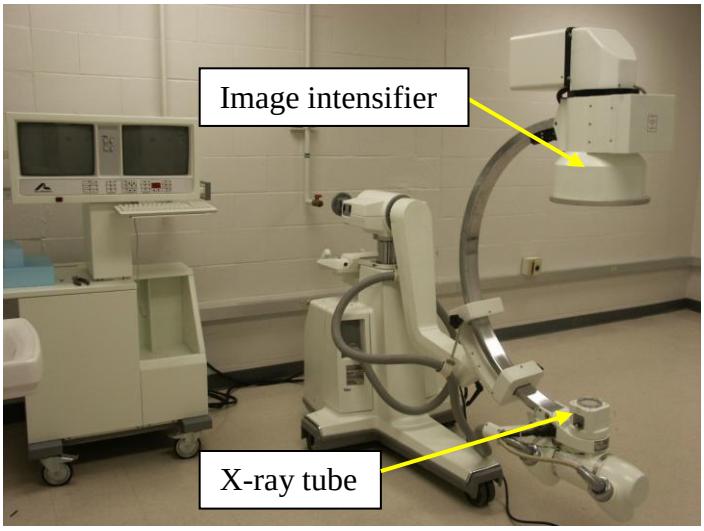

Figure 27. OEC Diasonics 9000 C-arm fluoroscopy X-ray unit

The laser source was then switched on at the lowest current setting (10 mA). To achieve a reliable current reading the thermistor resistance had to be set on the laser diode controller; 10 kΩ (25 ºC) were used as the operating temperature of the laser diode for our measurements. The diode controller was given a few seconds to reach the desired temperature, then the laser current was adjusted. The laser current was gradually increased to an erasing current of 600 mA. Although the maximum operating current of the diode controller was 1000 mA, in order to maximize the erasing performance and decrease the possibility of damage to the equipment 600 mA was used. The light diffuser was inserted into the hollow cylinder core of the storage phosphor tip and erasing was performed for 30 seconds. It was important to insert the laser diode into the hollow part of the storage phosphor tube rapidly in order to minimize the amount of erased signal before the laser diode was fully in position for the erasing experiment. After 30 seconds of erasing the laser light source was switched off and the erased storage phosphor tip was placed back in the light tight envelope.

Next the second tip was removed from the envelope and placed on a 30 Watt Porta trace flat panel light source. The light source was then switched on and the tip was erased for a period

of thirty seconds and placed back inside the envelope. The two tips were removed from the envelope in the dark room and were flattened. The flattened tips were simultaneously attached to the drum of the Perkin Elmer Cyclone storage phosphor readout system (Figure 28). As the drum rotated an optical laser scanned the surface of the drum and produced an image.

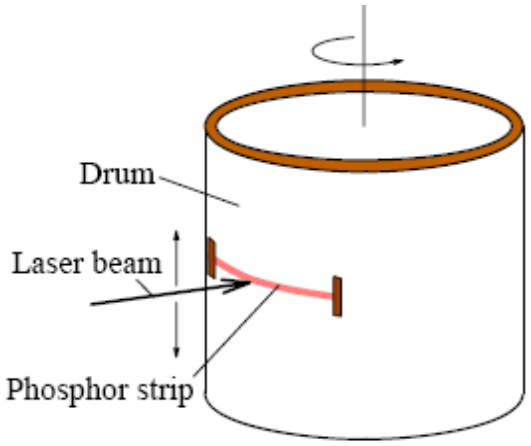

Figure 28. Schematic of storage phosphor readout system. Phosphor tip wrapped around the drum of the readout system. The drum rotates as the optical laser scans the surface of the storage phosphor detector tip.

The process of irradiation and readout was performed 9 times, increasing the erasing time by 30 seconds for each consecutive trial. The digitized images of the deposited signal were saved as Tiff files and processed using the ImageJ image processing software. All acquired images were transformed from 16 bit to 32 bit images. The pixel values within the images were squared in order to overcome the square root factor which was used to display images by the Cyclone software. The residual signal following readout was tabulated and graphed using the Origin graphing software.

2.3.2 Simulating Patient Like Conditions

To simulate realistic conditions the phosphor strips were irradiated in a patient phantom. The patient phantom consisted of blocks of acrylic with a thickness of 1.3 cm each.

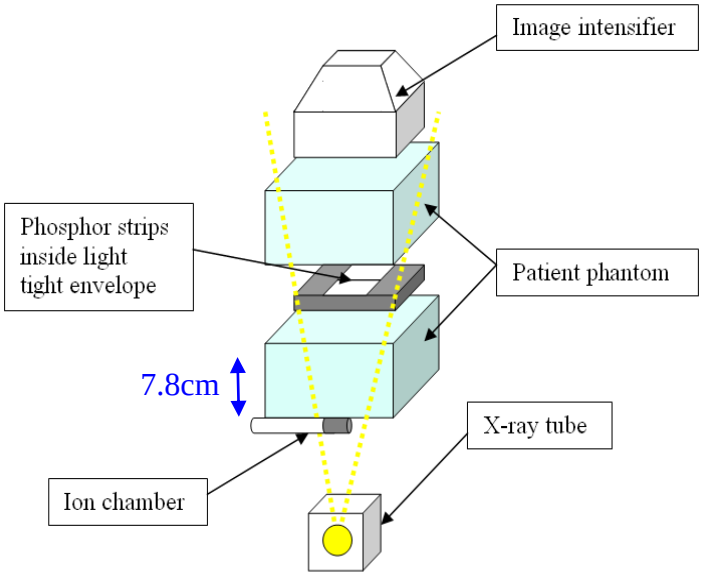

Figure 29. Schematic of imaging setup with acrylic patient phantom between the x-ray tube and the image intensifier.

Twelve blocks were stacked on top of each other the phosphor strips in the light tight envelope were placed between the 6th and 7th blocks (Figure 29). An ion chamber was placed directly adjacent the block closest to the x-ray source to monitor patient entrance dose. A lead collimator was placed above of the source to create an 8 cm by 8 cm rectangular field. Two storage phosphor strips were exposed to a 30 Watt Porta trace 1118 flat panel white light source for 10 minutes in order to reach background level conditions. The strips were then inserted inside a light tight envelope and placed in the gap between the acrylic blocks. Entrance exposure to the patient phantom was varied in correspondence to the radiation that was expected to be delivered to the storage phosphor strip during fluoroscopic guidance.

The experiment with the patient phantom was performed at entrance exposures of 100, 200, 400, 800 and 1600 mR. Once the strips inside the patient phantom were irradiated one of the strips was removed from the envelope in a dark room. It was then inserted inside a clear plastic tube in order for the strip to take on a cylindrical shape. The laser source was then switched on and the current was increased to a standard 600 mA in order to maximize the erasing

performance and minimize the possibility of damage to the equipment. Next the light diffuser was inserted into the hollow cylinder formed by the storage phosphor strip and erasing was performed for 2 minutes which represents the amount of time for erasing available during fluoroscopic insertion. After erasing the light source was switched off and the strip was placed back in the light tight envelope. The same process was performed with the unexposed strip remaining inside the light tight envelope. Once the two strips were erased they were simultaneously flattened and wrapped around the drum of the PerkinElmer Cyclone readout system. The readout was performed and the results were tabulated.

2.4 AIM 4: DETERMINING SNR FOR INTRAVASCULAR POSITRON AUTORADIOGRAPHY IN A HEART PHANTOM

In the preliminary studies [7] for the design of the storage phosphor detector tip, the four major factors determining the sensitivity of the detector were investigated. These four factors were: (1) fraction of positrons that have an initial direction toward the phosphor tip; (2) fraction of positrons that are absorbed in the blood surrounding the phosphor tip; (3) energy loss of positrons in the blood; and (4) Stopping power of the phosphor for positrons [7]. Although these aspects were only investigated analytically, so an experiment was devised to quantify the impact of these factors on the detectability of vulnerable plaque in. A heart phantom was designed and fabricated to model realistic conditions inside the coronary artery during vulnerable plaque imaging by storage phosphor detector tips.

The heart phantom (Figure 30) was fabricated from tissue equivalent acrylic (ρ =1.2 g cm^{-3}) as a cylinder with outer diameter of 82.25 mm. The inner diameter was 69.40 mm. The cylinder wall was 12.85 mm. The external height of the acrylic cylinder was 97.20 mm. This shape of the phantom approximately simulates human heart and it has a myocardial tissue volume similar to the human heart. An acrylic circle of 69.40 mm diameter and 4 mm thickness

sealed one end of the hollow cylinder. The circle was epoxied to the cylinder, making it water tight from one end. The cylinder's inner volume was 367.7 mL, similar to the average volume of the human heart which is approximately 300 mL. Additionally four channels were cut into the wall of the cylinder, running parallel to the cylinder axis and evenly spaced around the circumference. The depth of each channel was 3.15 mm and the width was 3.93 mm. The length of each channel was 90.16 mm. The purpose of the channels was to create slots for plastic tubes that would simulate the coronary arteries. This design allowed measurements in four "coronary arteries" at a time.

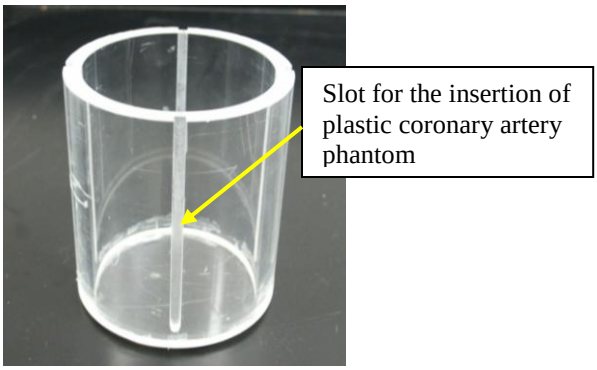

Figure 30. Acrylic heart phantom with grooves for simulated coronary arteries.

Along with the storage phosphor assembly, 0.5 x10^{-3} μCi mm^{-3} FDG solution filled each tube to simulate blood. The inner diameter of the plastic tube was 3.12 mm in comparison with the 2 mm diameter of the storage phosphor detector assembly. This allowed for a volume of 0.134 mL of FDG solution to fill the artery phantom. The tube was long enough to fit the entire length of the artery channel. The tube also had to be water resistant to prevent the FDG solution from leaking out. Heat resistance was important for the tubes not to melt or deform during the application of heat to their outside surface for the purpose to expedite the drying of the FDG solution deposited on the porous silica plaque phantoms. The bottom of each tube was plugged with a piece of aluminum of circular cross section. The diameter of the aluminum plugs was

3.16 mm. This was slightly larger than the diameter of the tube, however the elasticity of the tube allowed for the plug to fit and seal the bottom of the tube.

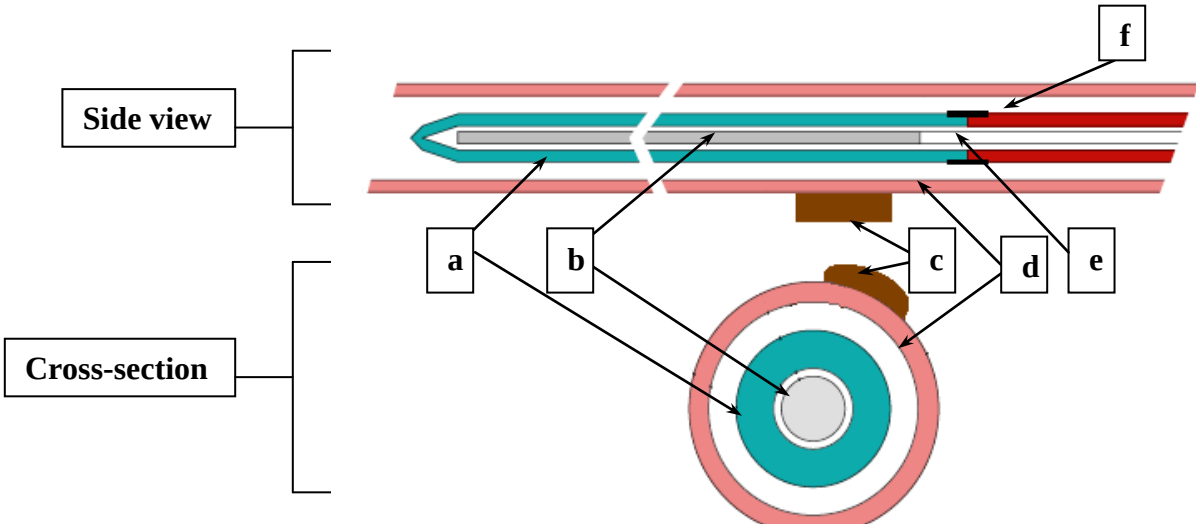

Figure 31. Components of storage phosphor detector assembly: (a) phosphor tip; (b) light diffuser; (c) coronary artery plaque phantom; (d) artery phantom wall; (e) optical fiber; (f) catheter tube

Due to the relatively short range of positrons in tissue and blood, the amount of material between the positron source (plaque phantom) and the detector (storage phosphor tip) had to be minimized. The coronary artery tube posed one of the primary obstructions in the path of the positrons. Because the source of radiation was going to be located on the outside of the tube during the detection process (Figure 31), a fraction of the positrons would get absorbed in the tube material. For this reason the tubes had to meet specifications for wall thickness, diameter, adequate length, heat resistance, water resistance and rigidity. The wall thickness of the tube had to be minimal in order for the positrons emitted from the plaque not to get absorbed inside the wall. The wall thickness of the tubes used in this experiment was 0.13 mm. The diameter of the tube had to be sufficient to fit the phosphor tip, light diffuser, catheter tube and the clear plastic sheath covering the assembly.

The next step in fabricating a heart phantom entailed modeling the coronary artery plaque. The average surface area of coronary artery plaque was estimated to be 10-20 mm^2 [7]. To simulate the uptake of FDG within vulnerable plaque inside the coronary artery, a material had to be chosen to imitate the characteristics of the plaque filled with FDG. A thin sheet of porous silica with a thickness of 0.38 mm with plastic base was chosen. Multiple rectangles with a surface area of 4x6 mm^2 were cut out. The porous silica layer was then separated from the plastic base layer using double sided clear adhesive tape, as previously described. The adhesive side of the rectangle was then attached to the artery tube so that the longer side of the rectangle was parallel to the length of the tube (Figure 32). The central point of the first rectangle was positioned 20 mm from the open end of the tube. The porous silica rectangle was gently wrapped around the wall of the tube to improve the geometry and increase the likelihood of positrons interacting with the detector. Two more porous silica squares were attached on the same tube with a spacing of approximately 15 mm. Care had to be taken to ensure that while wrapping the rectangles around the tube wall the porous silica material would not detach from the clear double sided tape.

To further improve source geometry a series of rubber squares were inserted into the channels to raise the position of the tube with respect to the bottom of the channel and to take

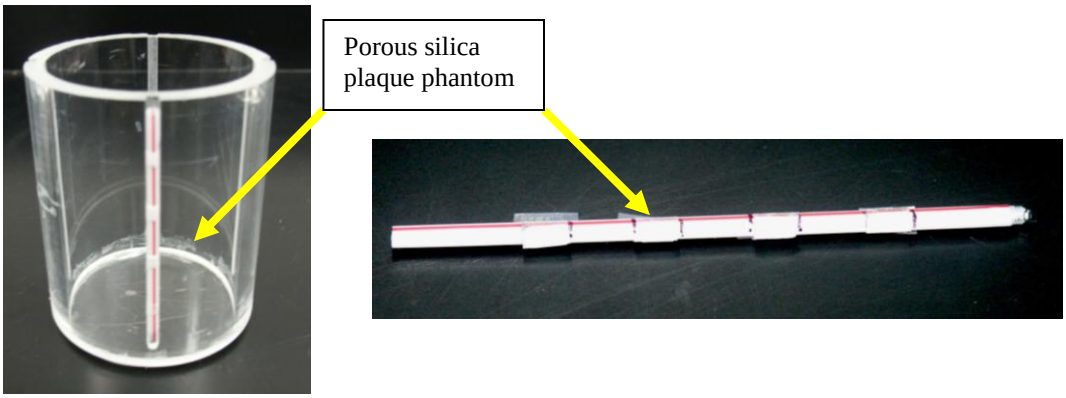

Figure 32. Acrylic heart phantom with plastic coronary artery tube and porous silica plaque phantoms.

better advantage of the arc created by the silica rectangles wrapped around the tube wall. Three rubber squares were inserted per channel at distances alternating with the position of the porous silica rectangles in order for the squares not to interfere with the rectangles. The entire assembly was then fastened to the acrylic cylinder with three pieces of clear adhesive tape at the top, center and bottom of the tube. An FDG solution was diluted with water to produce four activity concentrations: 40, 20, 10, and 2 x10^{-3} μCi mm^{-3}. Each of the four porous silica rectangles received 4 mm^3 of one of the solutions (Figure 33). Each of the four tubes had one square of

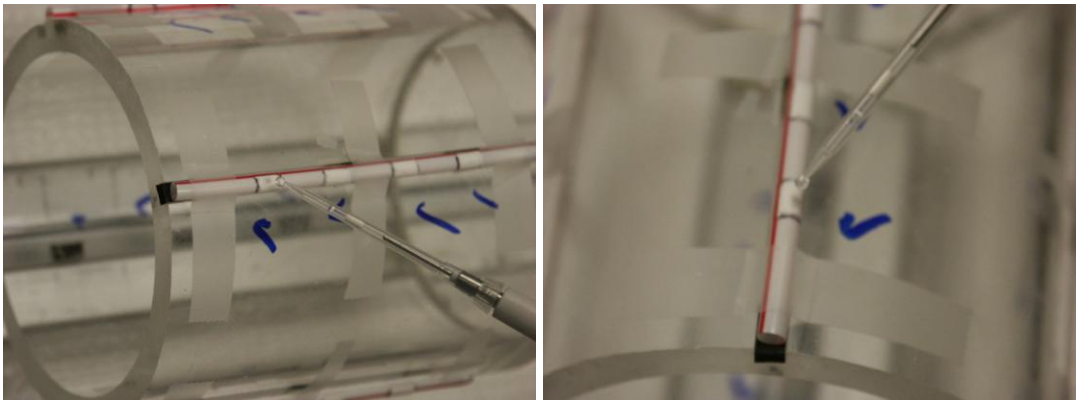

Figure 33: Deposition of FDG onto porous silica coronary artery plaque phantoms. Volume of FDG = 4 mm^3.

each activity. After deposition, each rectangle was dried with a heat gun (Alpha Wire company MG-1 Heat gun 360 W) for a period of less than 1 minute (Figure 34).

Additional FDG solution was emptied into a 50 mL volumetric flask; the volume error for the flask was +/- 0.05 mL. Decay correction was then performed to determine the amount of activity remaining in the beaker at the estimated time of data acquisition. The beaker was then filled with water to achieve an activity concentration that would decay to 0.5 x 10^{-3} μCi mm^{-3}at the time of data acquisition. After mixing, 300 mL of this solution was transferred into the acrylic cylinder modeling the myocardium.

The plastic tubes were also filled with the 0.5 µCi, using an epidural needle (Figure 35) and syringe, after insertion of the detector assembly into the tube. Care was taken to place the tip of the needle at the bottom of the plastic tube during filling to avoid trapping air bubbles in the plastic tube.

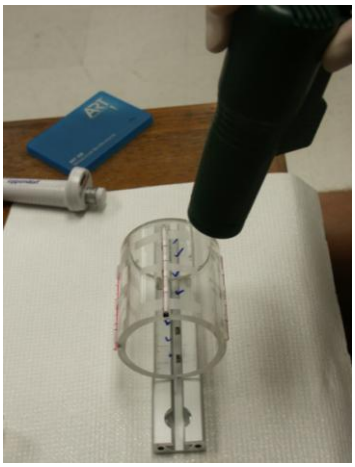

Figure 34. Epidural needle for filling the coronary artery tubes with low concentration FDG solution.

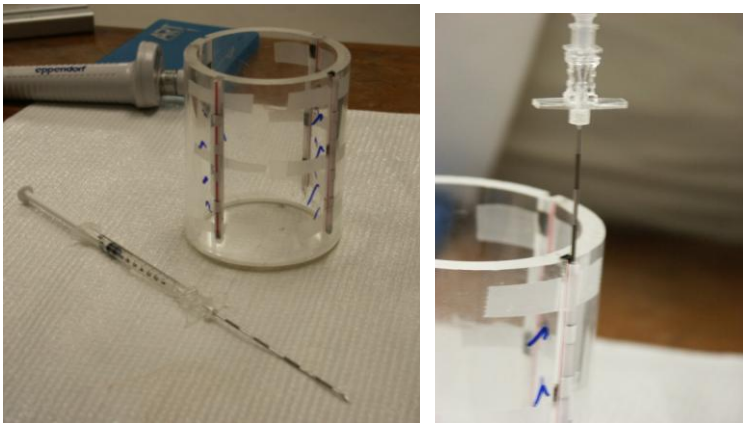

Figure 35. Drying of porous silica squares with heat gun.

2.5 AIM 5: DETERMINE THE IMPACT OF SCATTERED GAMMA PHOTONS ON THE PURE BETA SIGNAL COLLECTED FROM THE CORONARY ARTERY PLAQUE

Storage phosphor materials are sensitive to photons as well as positrons. In the current application only positron signal is desired so the amount of signal due to annihilation photon interactions must be assessed. Even though the contribution of annihilation photons to the background signal was shown to be small [16], it must be quantified here for inclusion in signal to noise ratio calculations. Fluorine-18, the source of radioactivity in FDG decays via the process of positron decay. In this process a proton in the nucleus is transformed into a neutron and a positively charged antiparticle of the electron. The positron and a neutrino are ejected from the nucleus. After ejection from the nucleus, the positron loses its kinetic energy in collisions with atoms of the surrounding matter, travelling no more than a few millimeters from the site of its origin in body tissues. The positron and an electron for a short period of time form an "atom" called positronium, which has the positron as its "nucleus" and a lifetime of about 10^{-10} seconds. The positron then combines with the electron in an annihilation reaction, in which their masses are converted into energy. The mass energy equivalent of each particle is 0.511 MeV. This energy appears in the form of two 0.511 MeV annihilation photons, which leave the site of the annihilation in exact opposite directions [8].

To measure the contribution of annihilation photons to background signal in a storage phosphor detector, two experiments were performed. One experiment measured the amount of signal recorded as a result of detecting both annihilation photons and positrons. The other experiment measured the amount of signal recorded only from the annihilation photons.

FDG solution was diluted with water in a 500 mL beaker to produce an activity concentration, at the time of dilution that would decay to the target concentration of 0.5 x 10^{-3} μCi mm^{-3} at the time of data acquisition. The contents of the beaker were mixed and 300 mL of this solution was transferred into the heart phantom (Figure 36). Recall that 300 mL represents the volume of an average human heart. A 108.8 x 16.9 mm^2 strip was then cut out of a high sensitivity low resolution Kodak storage phosphor plate.

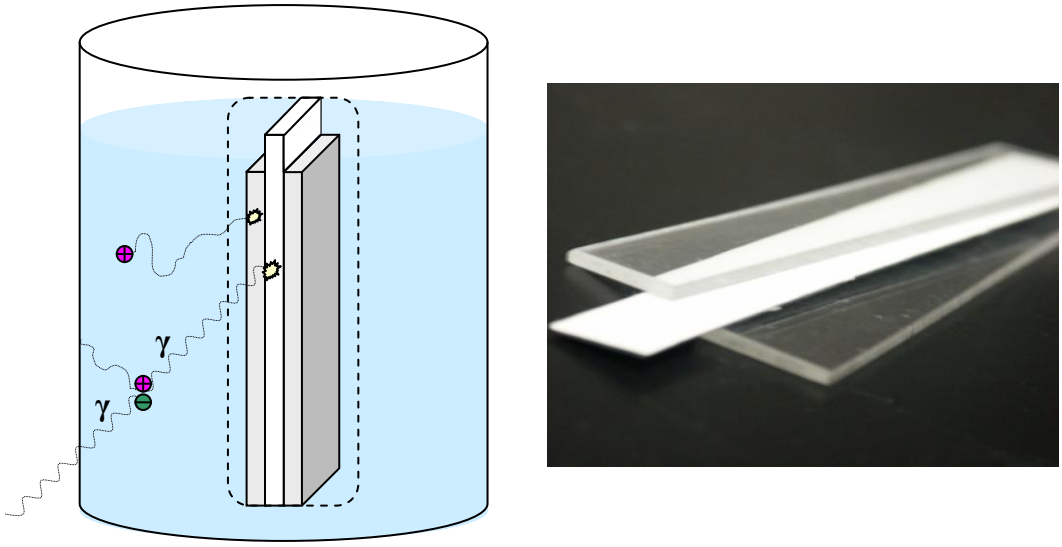

Figure 36. (left) Illustration of the experimental setup, with the storage phosphor detector sandwiched between acrylic plates and immersed in FDG solution. The red "+" represents positrons, the green "-" represents electrons and the "γ" represents photons. Positrons cannot reach the storage phosphor strip, photons can. (right) Photo of phosphor strip with the acrylic plates.

Prior to each experiment, the strip was exposed to white light for an erasing period of 10 minutes to remove any residual signal. The average range of positrons in blood is 0.6 mm. At the end of this track the positron interacts with a free electron and the positron electron pair annihilates. During the annihilation process a pair of photons is created with directions approximately 180º from each other and both photons have an energy of 0.511 MeV To measure the pure photon contribution to the signal from gathered during data acquisition, the storage

phosphor strip was sandwiched between two acrylic plates and inserted inside a, clear plastic envelope with a wall thickness of 0.05 mm. The two thin acrylic plates (100.6 x 20.1 x 2.29 mm^3), slightly wider than the storage phosphor tips, were cut out from a large sheet of acrylic (Figure 36). The plastic envelope with the storage phosphor strip was then immersed for 2 minutes in the 0.5 x 10^{-3} μCi mm^{-3} FDG solution inside the 300 mL heart phantom (Fig 37). Because the maximum range of ^{18}F positrons is 2.3 mm, the two acrylic plates shielded the

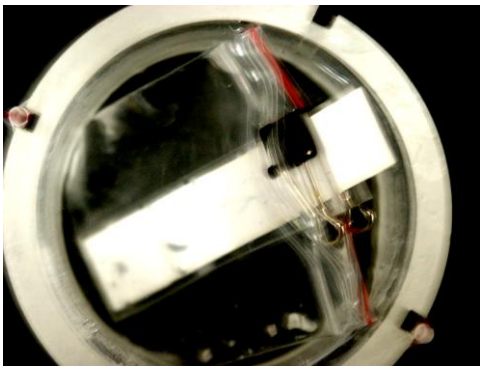

Figure 37: Storage phosphor strip sandwiched between two acrylic sheets, enclosed in a plastic water tight envelope, submerged in 0.5 x10^{-3} μCi mm^{-3} FDG solution

storage phosphor strip from incoming positrons; they were absorbed inside the acrylic before breaching the storage phosphor strip. After 2 minutes, the storage phosphor strip was removed and stored in a light tight envelope, while the phantom was removed from the dark room. The strip subsequently was wrapped around the drum of the Perkin Elmer Cyclone storage phosphor readout system and subsequently read out, as described previously.

To measure the background photon signal along with the desired positron signal on the storage phosphor strip, only one acrylic plate was used (Figure 38). The acrylic plate was placed adjacent to the side of the strip with the flexible support layer covering the back side of the phosphor layer, and the strip and plate were inserted in the plastic envelope. This technique was

used to only expose the side of the strip with the storage phosphor material. The strip was erased for 10 minutes. The plastic envelope was placed in the 0.5 x10^{-3} μCi mm^{-3} FDG solution inside the heart phantom. The room was darkened and data was acquired for 2 minutes. After 2 minutes, the storage phosphor strip was removed and stored in a light tight envelope, while the phantom was removed from the dark room. The strip subsequently was taken out of the light tight envelope, wrapped around the drum of the Perkin Elmer Cyclone storage phosphor readout system and read out. The two experiments took place in succession to keep the activity concentration inside the beaker relatively constant with respect to time decay.

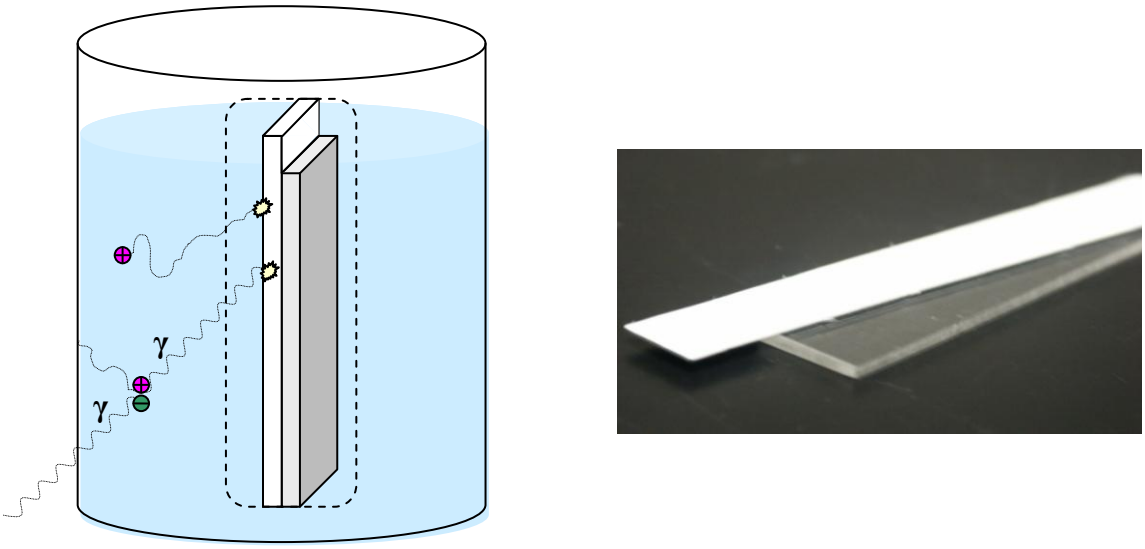

Figure 38. Positrons and annihilation photons detected on storage phosphor strip (right). Storage phosphor strip with a thin acrylic sheet for measurement of the sum of positron and scattered gamma contribution to background signal (right).

After the experiments a spreadsheet was developed to determine the exact activity concentration inside the beaker during the experiment with respect to the original activity determined by the dose calibrator. The final activity concentration during data acquisition was determined by the exponential time decay relationship (equation 1).

The digitized images were saved as .TIFF files and transferred into the ImageJ image analysis software. Plot profiles were taken of both strip images in the longitudinal direction.

CHAPTER 3 RESULTS AND DISCUSSION

This chapter presents the results of the following experiments enumerated in Chapter 2. The results of the experiments involved in fabricating the storage phosphor detector tip are in Section 3.1. Section 3.2 gives the results of determining the detectable range of activity concentrations. The erasing efficiency of the storage phosphor system is presented in Section 3.3, while the results of the experiments testing the performance of the storage phosphor detector in patient like conditions using a heart phantom are in Section 3.4. Finally the contribution of annihilation photns compared to positron signal collected from coronary artery plaque is discussed in Section 3.5.

3.1 STORAGE PHOSPHOR TIP FABRICATION

The storage phosphor detector tip required for positron autoradiography of the inside of the coronary artery was fabricated to meet functionality criteria while not creating a lethal obstruction inside the coronary artery. The overall length of the storage phosphor detector tip was 5 cm which corresponds to the average length of the human coronary artery. The detector material was obtained by separating the storage phosphor layer from commercially available high sensitivity, low resolution storage phosphor plates. Due to the fragility of the storage phosphor crystal material and the limited availability of sophisticated equipment the resulting cylindrical detector had a rectangular cross section instead of a circular one. This decreased the spatial resolution and field of view of the detector as opposed to the one proposed with a cylindrical shape. Having four storage phosphor segments however proved to be sufficient for the detection of activity concentrations needed for the imaging of human coronary artery plaque.

3.2 DETECTABLE RANGE OF ACTIVITY CONCENTRATIONS

The most reliable results in the process of determining the range of detectable activity concentrations were derived from using the natural decay of Fluorine-18 as opposed to diluting a high concentration of the solution. Although this process was time consuming due to the relatively long half life of ^{18}F, it provided a reliable qualitative and quantitative scale for the absolute detectability of a wide array of activity concentrations. Figure 39 shows the image obtained by repeated measurements spanning the decay of the FDG deposited on the porous silica squares. Two high activity concentration solutions were deposited on the porous silica squares located in the first two rows of the first column. The activity concentration contained within these two porous silica squares was identical in order to improve the confidence in the results of the experiment. The two porous silica squares in the bottom two rows of the first column were filled with medium activity concentration FDG solutions. The activity concentration contained in the two porous silica squares was identical, however by using a second set of activity concentrations the amount of information gathered throughout the experiment was doubled. This way the decay process was imaged for two different activity concentrations of FDG after the duration of each half life. The data set from the second column was not included in the results section due to measurement error. During data acquisition the plate was not moved after the two minute exposure, therefore data was collected from two different activity concentrations at the same location on the plate. This resulted in signal readout that was higher than that anticipated based on the natural decay of FDG. The data point in the third column was obtained immediately after the second 2 minute exposure in the second column, therefore that point corresponds to the correct activity concentration. The anticipated activity concentrations were calculated according to time dependent exponential decay.

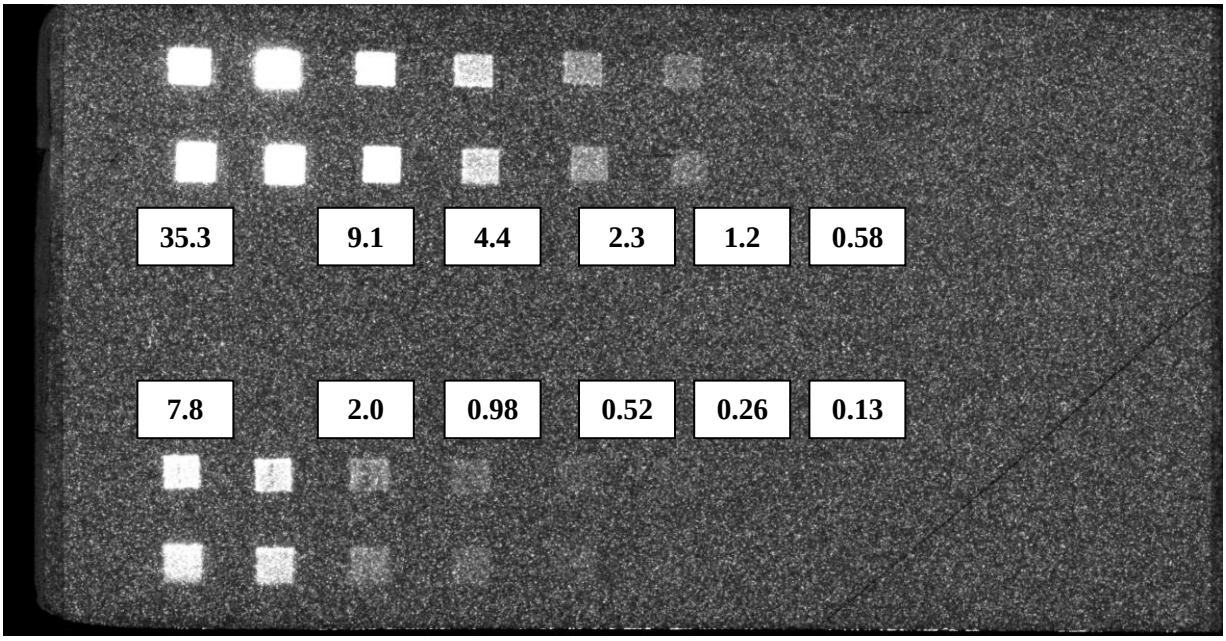

Figure 39. Signal detected by conventional storage phosphor plate during the decay of ^{18}F in FDG solutions deposited on porous silica squares. Each acquisition for two minutes at intervals of 110 minutes. The activity concentrations are expressed in $x10^{-3}$ μCi mm^{-3}. Data omitted from second column for operator error.

The raw signal deposited by the individual porous silica squares displayed in Figure 40 was clipped from the image and summed with the anticipated scattered gamma background signal obtained throughout the project. The squares were sorted according to decreasing activity concentrations deposited on the porous silica squares. The sequence of activity concentrations is displayed in Figure 40.

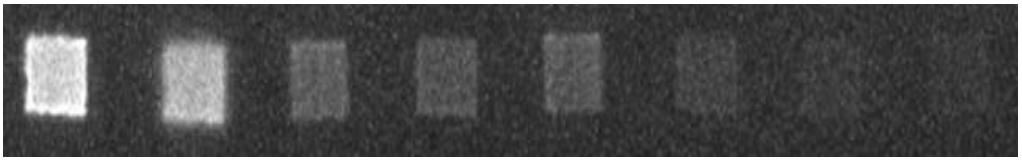

Figure 40. Range of detectable activity concentrations stacked on top of background signal coming from both positrons and scattered gamma photons. Image created by patching together the individual images obtained during data acquisition. The activity concentrations from left to right were 35. $x10^{-3}$ μCi mm^{-3}, 18.2 $x10^{-3}$ μCi mm^{-3}, 7.8 $x10^{-3}$ μCi mm^{-3}, 4.4 $x10^{-3}$ μCi mm^{-3}, 4.0 $x10^{-3}$ μCi mm^{-3}, 2.3 $x10^{-3}$ μCi mm^{-3}, 1.2 $x10^{-3}$ μCi mm^{-3}, and 0.98 $x10^{-3}$ μCi mm^{-3}.

In comparison to the data generated via the process of exponential decay, the results using dilution converge at higher activity concentrations (Figure 41). The reason for this discrepancy in the data has been attributed mostly to the lack of control over the amount of solution deposited on the porous silica squares. A 1mL syringe was used for the deposition of the FDG solution making it difficult to keep the volume of the deposited amount constant. For this inaccuracy in our measurements the data from the exponential decay experiment was used for determining the absolute detectable activity concentration. The magnitude of the horizontal error bars was determined based on the errors associated with the dilution process. The individual error contributions are described in the methods section. The following equation was used to determine the mechanical measurement error contribution.

$$\left(\frac{\sigma_u}{u}\right)^2 = \left(\frac{\sigma_x}{x}\right)^2 + \left(\frac{\sigma_y}{y}\right)^2$$

Equation 2. Error equation for determining mechanical error during the dilution process

In equation 2 σ_u represents the total mechanical error due to dilution, σ_x represents the error associated with volume and σ_y represents the error associated with the dose calibrator.

The derived equation for mechanical error had the following form.

$$\sigma_u = u\sqrt{\left(\frac{\sigma_x}{x}\right)^2 + \left(\frac{\sigma_y}{y}\right)^2}$$

Equation 3. Derived equation for determining mechanical error during the dilution process

The vertical error bars represent the standard deviation of the pixel values within the ROI drawn around the image of the plaques. The size of the ROI corresponded to the area enclosed by the external perimeter of the smallest visible plaque image. The vertical error bars at lower activity

concentrations are larger than at higher activity concentration. At lower activity concentrations the variation of pixel values within the ROI fluctuates more than at higher activity concentrations.

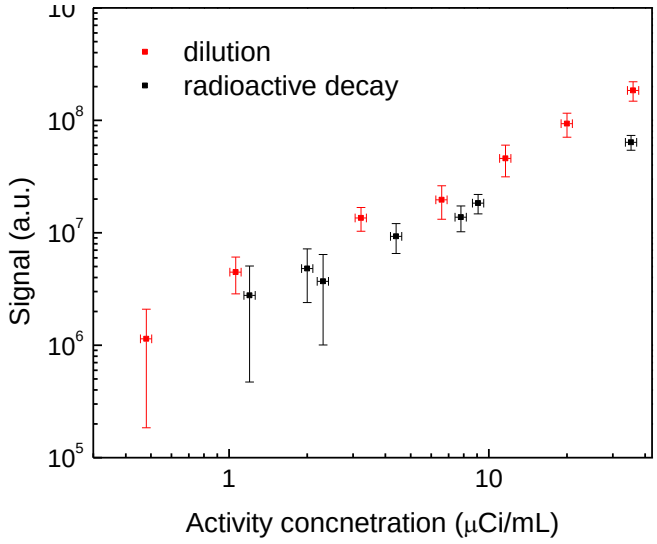

Figure 41. Comparison of signal values generated using the method of radioactive decay (black), and the method of dilutions (red).

For improved statistics two sets of data were taken simultaneously. The resulting data was tabulated and graphed. The measured background signal was subtracted from the mean plaque signal and was plotted against the activity concentration deposited on the porous silica square (Figure 42). The resultant curve follows a linear relationship up till the activity concentration of approximately 7.5 x10^{-3} μCi mm^{-3}. Both sets of data follow a similar trend. Data was generated using the ImageJ software. A region of interest was drawn around each image of porous silica square and the signal was averaged for each region of interest. The error bars associated with the x axis of this curve are partially attributed to dilution error, timing error and readout error. The error bars associated with the y axis are associated with the standard deviation of the pixel values with the region of interest. Error was calculated the same way as for the experiment with the two different dilution methods.

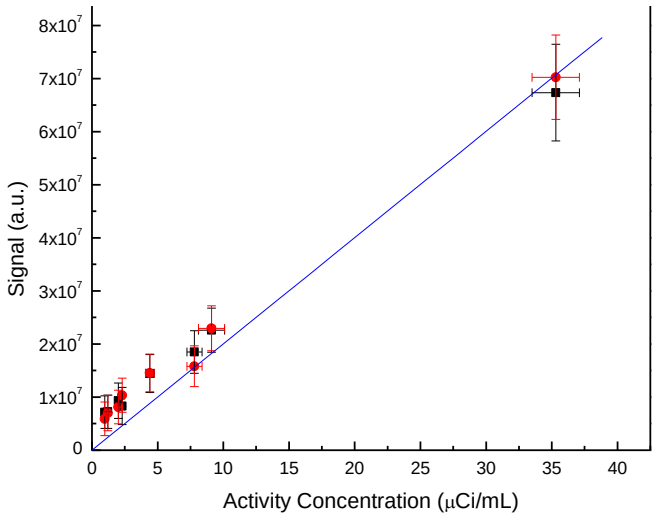

Figure 42. Plot of mean signal value with the background signal level subtracted as a function of Activity concentration. The two curves represent two separate sets of data gathered from the same storage phosphor plate.

The signal to noise ratio (SNR) was also calculated for the individual activities deposited on the porous silica squares. The method which was used for the quantification of SNR involved drawing a region of interest around the image of each artery plaque phantom square and averaging the signal. A region of interest of identical dimensions was also drawn around an area of the detecting medium outside of the perimeter of the plaque phantom image. The signal inside the background region of interest was also averaged. The standard deviation was calculated for the signal average of the region of interest surrounding the image of the artery plaque phantom. The following equation was used to determine SNR:

$$SNR = \frac{Signal - Background}{\sqrt{\sigma_{signal}^{\ 2} + \sigma_{background}^{\ 2}}}$$

Equation 4. Signal to noise ratio

The background signal in the equation represents the expected background signal level coming from gammas and positrons as opposed to actual noise. The image for the SNR determination

was synthesized using strips of storage phosphor images with signal levels corresponding to positron and gamma background in 0.5 x 10^{-3} μCi mm^{-3} activity concentration. This background was combined with the plaque phantom images obtained in the flat plate experiment. The SNR incorporates the difference in signal to background to composite noise. The determination of SNR in our case represents a conceptual approach. The stacked images did not allow us to draw conclusions about the detectability of plaque.

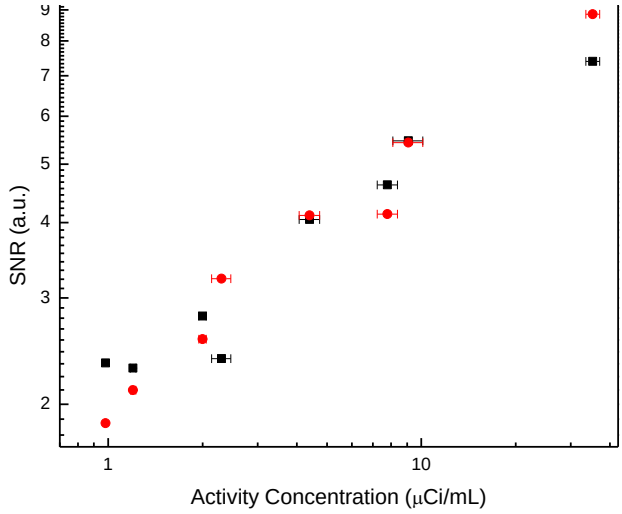

Figure 43. Plot of signal to noise ratio as a function of Activity concentration. The two curves represent two separate sets of data gathered from the same storage phosphor plate.

To determine the effectiveness of our detector system we used a modified version of the SNR analysis when the size of the contrast element was fixed at 6.5x6.5mm^2 and activity concentration was varied in the range of 0.13 x10^{-3} μCi $mm^{-3}$to 36 x10^{-3} μCi mm^{-3}. The reason for not varying the size of the contrast element was limited information available about sizes and shapes of the vulnerable coronary plaques. The postmortem autopsy studies have shown that the vulnerable coronary plaques may have complicated shapes and may extend up to 20-30 mm along the coronary artery. Also, it was technically difficult to produce simulated plaques with

sizes significantly smaller than 6.5 mm. Therefore, we have chosen the above size of the contrast element to perform initial analysis of the low contrast detectability.

The plot of signal to noise ratio as a function of deposited activity provides information on how easily the image of the porous silica plaque phantoms with FDG can be distinguished from background signal level. The high values of SNR for low activity concentrations (above 10) are representative of an ideal case, where the distance between the detector and the source is minimized and there is no absorber e.g. blood between the source and the detector that would interfere with the detectable positrons. This scale was created as a standard for the lowest detectable activity concentration for ideal conditions. The error bars associated with the data points represent the mechanical dilution error.

3.3 EVALUATION OF THE ERASING EFFICIENCY OF THE STORAGE PHOSPHOR SYSTEM

3.3.1 Erasing Efficiency Comparison of White and Red Light

The erasing efficiency of the storage phosphor system was evaluated for two types of light sources to determine whether white light with higher energy photons would reduce the signal level on the storage phosphor tip after irradiation as compared to the signal level after erasing with red laser light. In order to keep experimental conditions identical for both the red and white light sources, two storage phosphor tips were irradiated simultaneously. Data from previous experiments involving the same procedure only with the use of red laser light was also included. After irradiation and subsequent erasing, both tips were read out using the Perkin Elmer Cyclone readout system. The image was converted from a 16 bit image to a 32 bit image and saved as a TIFF file in ImageJ.

A region of interest was drawn encompassing the entire surface area of each tip and the average signal was recorded in correspondence to the amount of time the tip was exposed to the

erasing medium. The recorded signal was the square root of the actual signal, therefore before tabulating the data, the signal on the plate needed to be squared to obtain the actual pixel values on the plate. The square of the signal was plotted against the time of erasing. Erasing with the red light source had more data points at the lower end of the time scale because this method was studied more extensively due to its pertinence to our experiment. Data was taken for every 30 second erasing interval.

The expectation was to observe a level of divergence at long periods of erasing, making white light more effective at ejecting electrons from deeper traps, therefore decreasing the residual signal on the phosphor tip. The graph (Figure 44) shows a rapid decline of residual

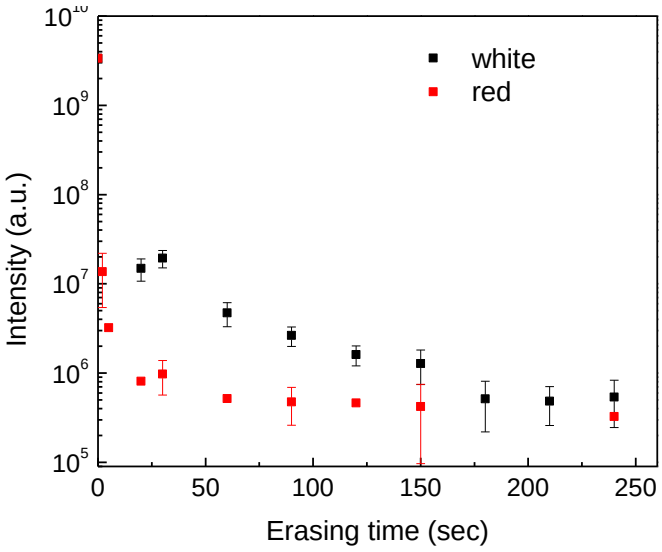

Figure 44. Erasing efficiency comparison of white and red light. Black box represents resulting signal levels with white light source. Red box represents resulting signal levels with red light source.

signal after short periods of erasing for the red laser erasing system, whereas the white light source residual signal declined more gradually. This was due to the lower intensity of white light; although the red light was lower in energy, its high intensity more efficiently removed electrons.

Increasing the time of erasing beyond 180 seconds for both light sources resulted in similar levels of residual signal converging at a constant background level. Fluctuations in intensity may have been caused by variations in X-ray output.

3.3.2 Erasing Experiment with Red Laser Light and Patient Phantom

The erasing of the storage phosphor tip is a continuous process during catheter insertion. It begins as soon as the first fluoroscopic photons are detected on the storage phosphor surface. It is estimated that the duration of the fluoroscopic insertion process is approximately 2 minutes [7]. Therefore 2 minutes was selected as the erasing time for the experiment while simulating patient like conditions. To improve statistics, two storage phosphor tips were used simultaneously throughout the procedure. The tips were irradiated inside a light tight envelope sandwiched between two layers of acrylic which simulated patient absorption. The entrance skin exposure was monitored with an ion chamber and was increased by a factor of 2 for each consecutive measurement. Measurements were taken at exposure levels of 100, 200, 400, 800 and 1600 mR.

The tips were irradiated, erased and read out simultaneously keeping the experimental conditions identical. After irradiation and subsequent erasing, both tips were read out using the Perkin Elmer Cyclone readout system. The image was converted from a 16 bit image to a 32 bit image, the pixel values were squared and the image was saved as a TIFF file in ImageJ.

A region of interest was drawn encompassing the entire surface area of each tip and the average signal was recorded in correspondence to the amount of exposure the given tip was subject to. The recorded signal was the square root of the actual signal, therefore when tabulating the data the signal from the Image J program needed to be squared.

While recording the signal data from the tips, a separate region of interest was drawn away from the tips encompassing areas that were subject to no radiation or erasing. This data was tabulated as electronics background. The resulting signal due to erasing during fluoro exposure for both tips was plotted against entrance skin exposure (Figure 45). With increasing

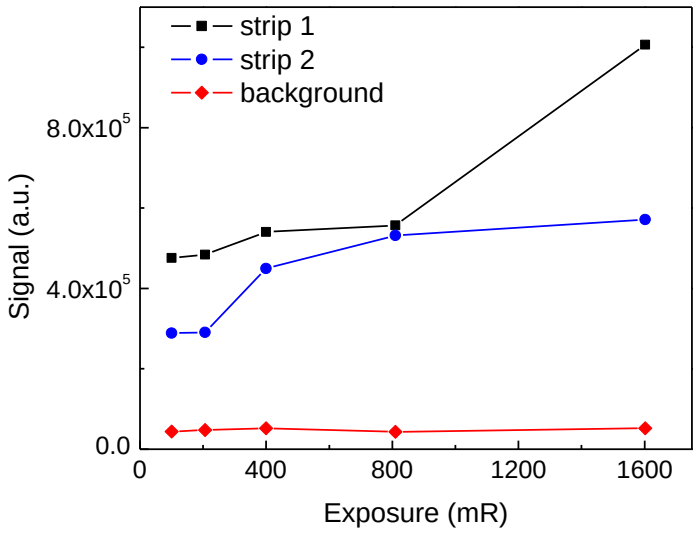

Figure 45. Patient entrance exposure vs. residual signal after two minute erasing

entrance exposure both graphs show increasing signal. Although there is divergence between the two graphs at higher entrance skin exposures, when compared to the dose deposited on the tips during fluoro-guided insertion residual signal level after erasing is negligible. The lowest plaque signal detectable by our system was at least two orders of magnitude higher than the highest residual signal from erasing during fluoro-guided insertion.

3.4 RESULTS WITH ACRYLIC HEART PHANTOM MODELLING REALISTIC CONDITIONS FOR BETA AND SCATTERED RADIATION DETECTION

The heart phantom was constructed out of patient equivalent material to imitate the volume and shape of the average human heart. The specifications of the heart construction

method and procedure are explained in detail in the methods and materials section. Multiple measurements and experiments were performed with the heart phantom to gather qualitative and quantitative results regarding the appropriateness of the experimental setup and the usefulness of the detector.

After a set of preliminary experiments a method was developed for the imaging of the activity concentrations inside the coronary artery plaque phantoms with reproducible results. To ensure that activity was present on the coronary artery plaque phantoms, a storage phosphor tip was held against the side of the coronary artery tube which contained the artery plaque phantoms, prior to the insertion of low concentration FDG solution into the heart phantom and the artery tubes. The qualitative results of the images, without accounting for absorption of detectable positrons in the low concentration FDG solution, produced an image of the four activity concentrations deposited on the porous silica plaque phantoms (Figure 46, 47). The

Figure 46. Image of storage phosphor strip flattened and held against artery plaque phantoms for a 2 minute acquisition time. The size of each plaque phantom was 4 x 6 mm^2, the volume of FDG deposited was $4mm^3$ and the activities from left to right were 4.0 nCi, 12.8 nCi, 38.6 nCi, 126.4 nCi. Arrows indicate damage to the phosphor layer, likely due to handling while putting the flattened tips on the readout drum.

image of each plaque phantom is easily distinguishable from the background signal. The above images represent an ideal case that could be achieved in vivo only if the coronary artery were drained and the detector were pressed up flush against the wall of the coronary artery. The fragility of the phosphor tips is evident from the defects in figure 46 and figure 47; this may be attributed to the handling of the storage phosphor tip in the dark and transferring it from the heart

phantom to the readout system drum. The activity concentrations on these simulated plaques were in the range from 0. x10^{-3} μCi $mm^{-3}$to 39.2 x10^{-3} μCi mm^{-3}.

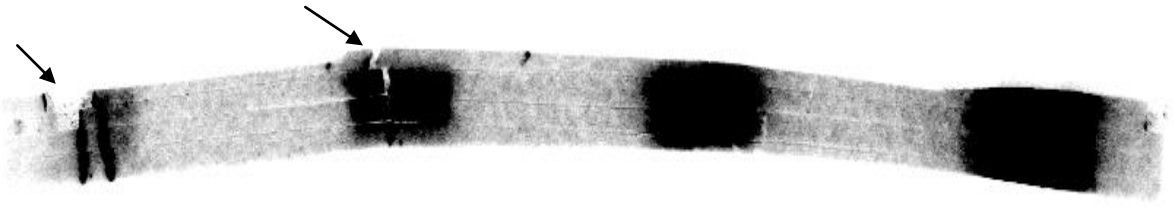

Figure 47. Image of storage phosphor strip flattened and held against artery plaque phantoms for a 2 minute acquisition time. The size of each plaque phantom was 4 x 6 mm, the volume of FDG deposited was 4 mm^3 and the activities from left to right were 4.0 nCi, 12..8 nCi, 38.6 nCi, 126.4 nCi. Arrows indicate damage to the phosphor layer, likely due to handling while putting the flattened tips on the readout drum.

The quantitative results for the above images are presented in the form of graphs relating the activity concentration inside the coronary artery to the signal read out by the storage phosphor readout system. The raw data from the readout software is squared on the ordinate in order to compensate for square root factor within the readout software. The plot of signal vs. activity concentration in this case resembles a linear relationship (Figure 48). The data points were generated by drawing a region of interest around the image of the artery plaque phantom. The signal was averaged over the region of interest and plotted against the activity concentration.

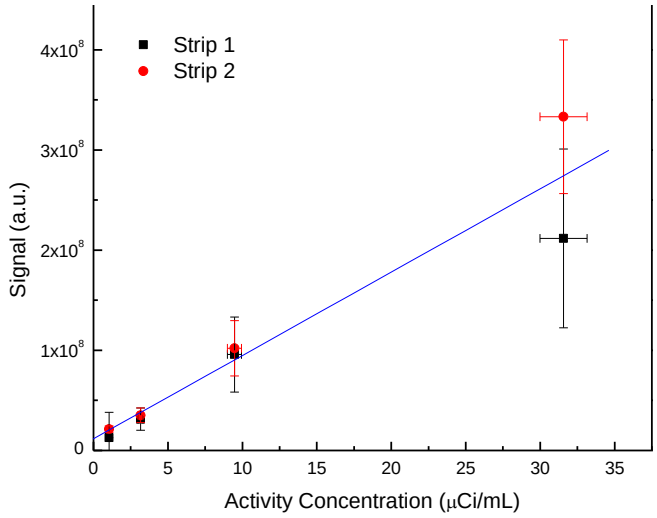

Figure 48: Activity concentration vs. signal, deposited on the flattened storage phosphor tip

The results of the experiments with the heart phantom and artery tubes filled with low activity concentration FDG solution are summarized in the following graphs (figure 49). Data was taken in two different trials which produced two sets of results with four tips in each trial. The first set of trials involved a wide range of activity concentrations ranging from 0.2 to 80 $x10^{-3}$ μCi mm^{-3}. The reason for encompassing a large array of activity concentrations was to gain a means of relating activity concentration to detectable signal. It is evident from the graphs that without low concentration FDG solution between the detector and the source the relationship between activity concentration and signal follows a linear pattern which corresponds to the predicted relationship. Compared to the case where the flat detector tips were held adjacent to the coronary artery tube with the plaque phantoms, the distance of the detector from the wall of the coronary artery was not as uniform therefore there is a level of deviation from an ideal linear relationship. Having some parts of the detector closer to plaque phantoms with lower activities pertaining to their neighbors with a higher activity concentration or vice versa may have caused the signal pertaining to those plaque phantoms appear higher than the signal The results presented in figure 50 represent the data obtained during the second trial of the above experiment. The experimental conditions were unchanged except for the activity concentrations which were focused on lower values that were closer to the activity concentrations anticipated from vulnerable plaques. The activity concentrations ranged from 0.07 to 40 $x10^{-3}$ μCi mm^{-3}.

After the image acquisition of the ideal tips without absorption within the low concentration FDG solution around the storage phosphor tip, the coronary artery tubes and the heart phantom were filled with low activity concentration FDG solution. One tip enclosed in a sturdy, plastic sheet was placed inside each of the four coronary artery tubes for the imaging of vulnerable plaque in a realistic condition. The total image acquisition lasted 2 minutes after which the tips were removed from the tubes and read out using the Perkin Elmer Cyclone storage

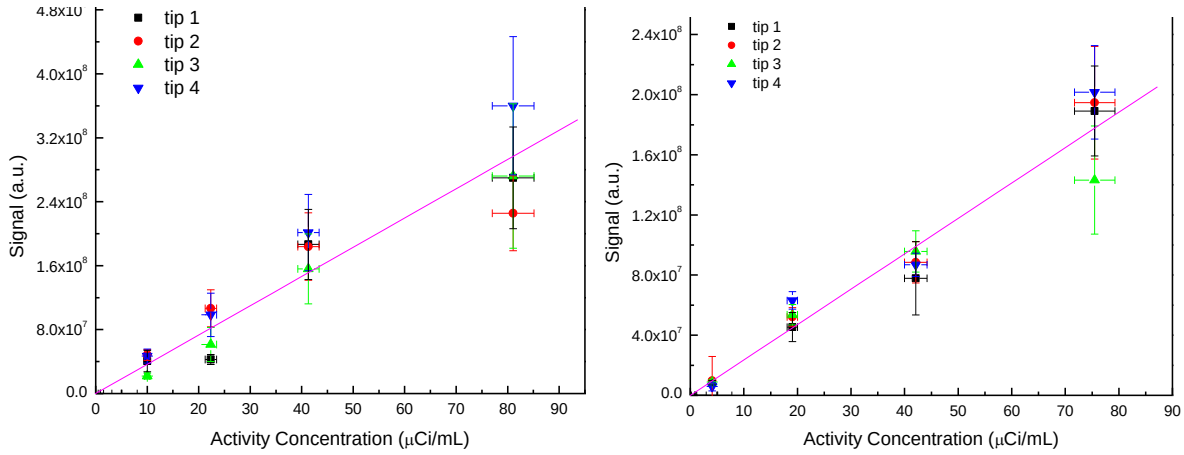

Figure 49: Results of imaging plaque phantom with detector tips inserted in artery tubes; no background activity was present. Results for 4 tips are graphed for each trial of the experiment.

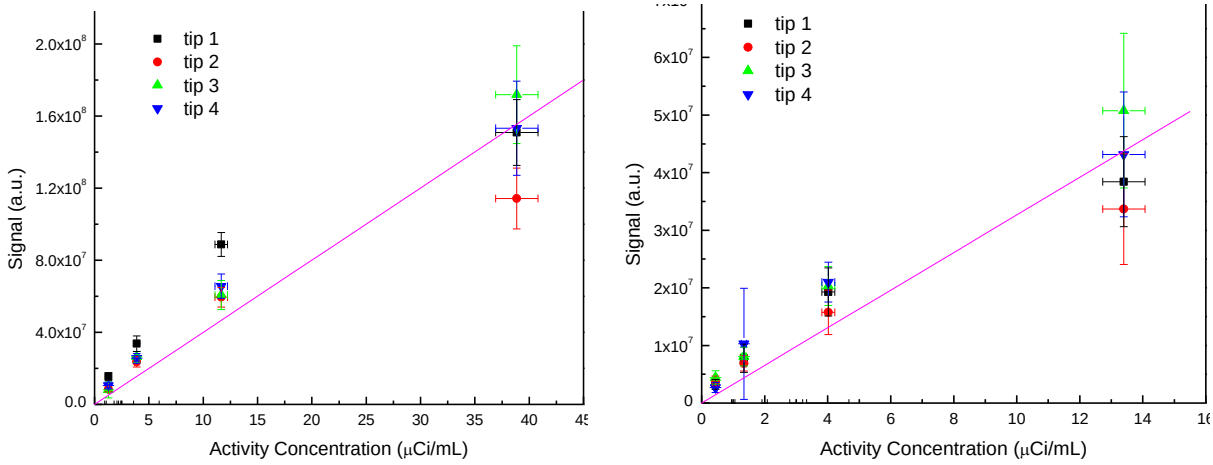

Figure 50: Tip results from trial two without low concentration FDG solution in heart phantom. Results for 4 tips are graphed for each trial of the experiment.

phosphor readout system. The pixel values in the image were squared using the ImageJ software to eliminate the square root factor in the readout software. Also to increase the signal to noise ratio the images were binned using larger pixel sizes. As a result three of the four plaque phantom images can be distinguished from background levels with the naked eye. Figures 51 and 52 represent the best qualitative results achievable with the current experimental setup and available fabrication tools.

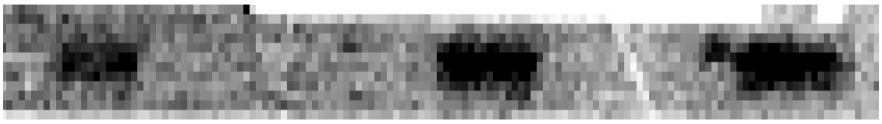

Figure 51. Image of storage phosphor strip inserted inside coronary artery tube for 2 minute acquisition time. Low concentration FDG solution was present in the heart phantom artery tubes. The size of each plaque phantom was 4 x 6 mm^2 and the activities from left to right are
4.2 nCi, 12.64 nCi, 42.16 nCi.

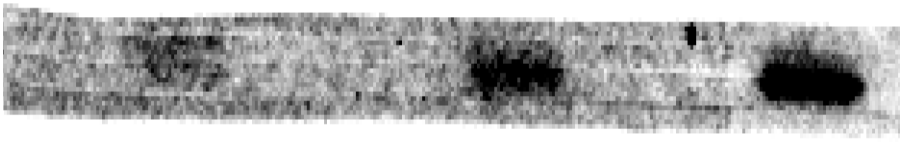

Figure 52. Image of storage phosphor strip inserted inside coronary artery tube for 2 minute acquisition time. Low concentration FDG solution was present in the heart phantom and artery tubes. The size of each plaque phantom was 4 x 6 mm^2 and the activities from left to right were 4.2 nCi, 12.64 nCi, 42.1 6nCi.

To provide a quantitative representation of the results from the experiments involving the absorption of positrons in the low activity concentration FDG solution surrounding the detector tip, the results were plotted for the four most successful trials. The resultant signal was plotted as a function of activity concentration. At lower activity concentrations the plot of the four tips shows agreement with a linear tendency up to approximately 5 $x10^{-3}$ $\mu Ci\ mm^{-3}$.

The plots below follow the layout of the experiments that did not use low concentration FDG solutions in the heart phantom and inside the coronary artery tubes. Due to positron absorption in the fluid in the artery tubes and gamma signal from the FDG solution in the tubes and the heart phantom, the resulting plots do not follow the patterns seen in figure 49 and figure 50. This behavior was predicted in preliminary studies. One of the main reasons for the change in the character of the graphs lies in the problem of keeping the distance of the detector from the artery tube wall constant. As the storage phosphor was inserted into the coronary artery tube there was no control which was exacerbated by the insertion of an epidural needle adjacent the phosphor tip to fill the tube with 0.5 $x10^{-3}$ $\mu Ci\ mm^{-3}$ FDG solution. For instance if the storage phosphor detector tip was inserted at a slight angle such that one end of the detector was closer to the low activity concentration plaque phantom then more positrons would be deposited on that part of the detector in comparison with the ideal situation when the distance would uniform. Results where higher activity concentration plaque phantoms provide a lower signal than their neighbors with lower activity concentrations are visible on the top two graphs in Figure 53.

The uncertainties involved in these results cannot be properly accounted for due to the lack of quantitative data generated during the testing of the heart phantom. The scope of this section was primarily the fabrication of the detector testing it in realistic conditions while generating preliminary results. Unfortunately many of the experiments were inconsequential or with contradictory data. During the procedure there was a lack of control over the distance of the detector from the coronary artery wall. Because the blood vessel cannot be completely blocked due to physiological reasons, it is impossible to get the detector directly adjacent to the coronary artery plaque. With varying distances a detector tip located closer to plaque with lower activity may be detected as plaque with more metabolic activity than plaque that has a higher activity concentration but is further from the wall of the coronary artery. This effect however may be

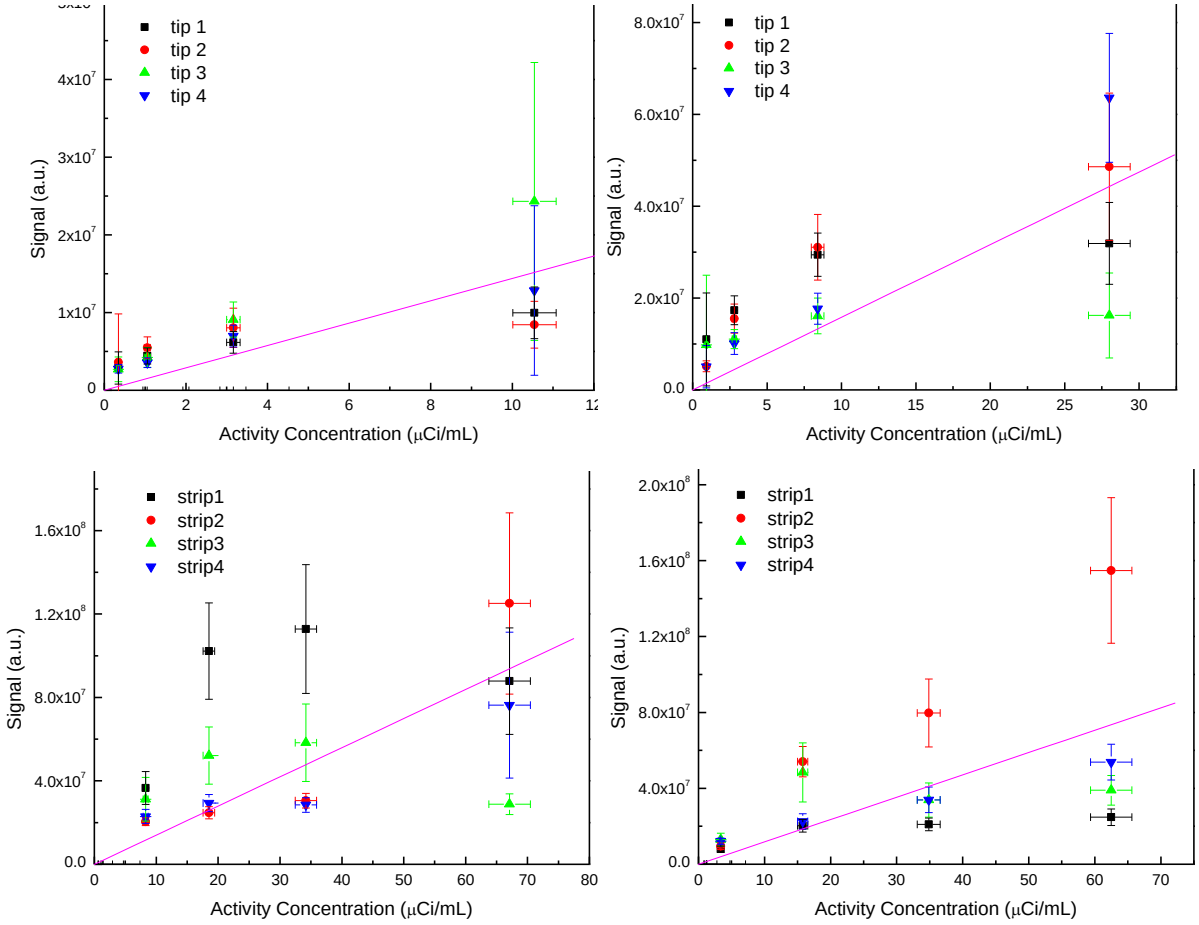

Figure 53. Plots resulting from trial 1 (top) and trial 2 (bottom) with low concentration FDG solutions present inside the heart phantom.

outbalanced by the fact that the plaque intrudes towards the lumen of the blood vessel. This is in contrast with our heart phantom which has the plaque phantoms positioned on the outside of the coronary artery tube. The phantom was designed like this because the porous silica material is not water resistant therefore if it were to come in contact with the low activity concentration FDG solution, the amount deposited on the plaque phantom would get contaminated with the low activity concentration FDG solution.

The absorption of positrons in blood affects the usefulness of the storage phosphor detector system. The signal however is calculated with respect to the distance from the vessel

wall which means that if the signal is weak, the background is also going to be weak relative to the signal, making it possible to distinguish the weak signal from the even weaker background.

3.5 THE IMPACT OF RADIOACTIVITY IN BLOOD AND HEART ON SIGNAL COLLECTED FROM THE CORONARY ARTERY PLAQUE

Two separate experiments were performed with a low concentration (0.5×10^{-3} $\mu Ci\ mm^{-3}$) FDG solution. The first experiment was aimed at determining the magnitude of the signal coming from scattered gamma photons in an environment with similar conditions to that inside the coronary artery after the injection of FDG into the artery. The concentration of the FDG solution in our experiment was the same as the expected concentration of FDG inside the coronary artery.

Signal was gathered using a storage phosphor strip over a period of two minutes with acrylic blocking the incoming positrons from being detected by the storage phosphor strip. The signal from the storage phosphor strip was subsequently read out the by the Perkin Elmer Cyclone storage phosphor readout system. The image was converted from 16 bit to 32 bit and saved as a TIFF file. A region of interest was drawn around the perimeter of the strip images and a plot profile was taken. The signal value for each pixel column was plotted against the distance in units of pixels from the origin of the plot profile boundary. The values for both the pure gamma signal and the sum of gamma and positron signal were plotted on the same graph to generate a qualitative measure of difference between the signal levels (Fig 54). The plot of the pure gamma signal decreases as we move further from the origin of the profile region. A possible explanation for this outcome is the increased backscatter from the dense table top to which the tip of the phosphor strip was closer during data acquisition. The relative distance on the plot may be interpreted as distance from the bottom of the beaker inside which the storage

phosphor strip was submerged in the low concentration FDG solution. Also positrons were not prevented from interacting with the storage phosphor strip at the bottom of the acrylic-storage phosphor sandwich because acrylic did not cover the portion of the bottom edge of the strip. For this reason positron contamination is also a likely cause of increased signal towards the bottom of the beaker.

It is evident from the graph that the combined signal from positrons and gammas is greater than the pure gamma signal, which means that positrons do generate signal in storage detectors. The average signal value for the pure gamma profile was 1.24 x 10^7 a. u. with a standard deviation of +/- 2.18 x 10^6 a u. The average signal value for the sum of the gamma and positron signal was 1.68 x 10^7 a. u. with a standard deviation of +/- 2.40 x10^6 a. u. According to this experiment the average value of the background signal within the low activity concentration FDG solution due to the contribution of scattered gammas and positrons is 1.63 times higher than

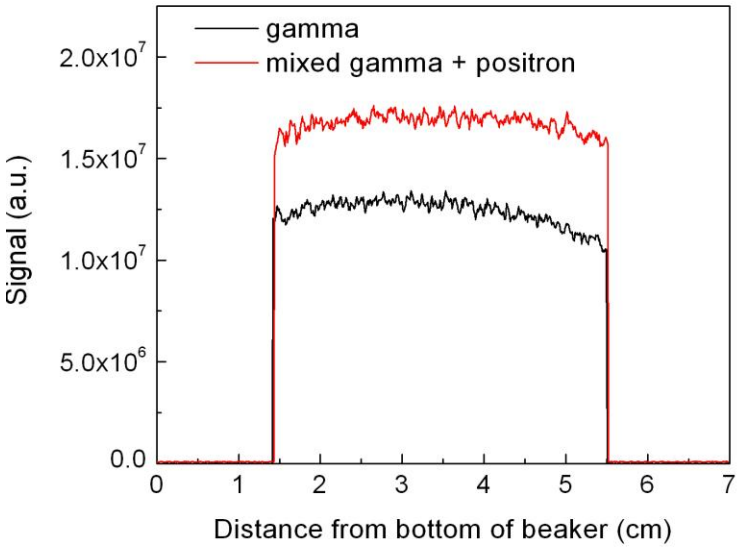

Figure 54. Comparison of pure gamma and mixed gamma + positron signals the average signal attributed only to the scattered gamma photons.

CHAPTER 4 CONCLUSIONS

The development of coronary artery plaque and the causes of the inflammation of the overlying endothelium have been studied extensively in multidisciplinary scientific fields. The increase of metabolic activity inside the inflamed cap covering the coronary artery plaque is an indicator which has the potential to provide quantifiable data about the risk of rupture. The Sokoloff model for the uptake of FDG in areas of higher metabolic activity provides a valuable method for imaging the accumulation of FDG in the inflamed part of the coronary artery plaque. Placing a particle detector directly adjacent to the wall of the coronary artery can directly detect positrons emitted by the accumulated FDG inside the plaque. The amount of FDG taken up by vulnerable coronary artery plaque has been studied in rabbits [14] that were sacrificed after the development of vulnerable plaques in the main arteries. Scaling the uptake value of FDG inside vulnerable plaque from rabbits to humans predicts that an intravascular FDG imaging system must detect at least the sensitivity sufficient for the detection of vulnerable plaques for humans is 40 nCi mm^{-2}[14].

The coronary artery plaques with 0.54 nCi mm^{-2} and 1.75 nCi mm^{-2} area activities with FDG solution as background were reliably imaged with storage phosphor detector. The plaque with 0.18 nCi mm^{-2} activity was difficult to visualize over the noisy background. Literature reports that human vulnerable plaques are expected to have average area activities of 40 nCi mm^{-2}. Therefore, our detector can image plaques with activities by a factor of 20-70 lower than required.

By increasing the diameter of the storage phosphor detector tip the detection of a larger number of positrons is possible by putting the detector closer within the average positron range and by lessening the absorption of positrons in blood surrounding the detector. The diameter of

the detector however may only be increased to a level that does not create a lethal obstruction in the artery. The distance between the detector and plaque phantom varied throughout our experiments which may account for some of the results that predict a plaque phantom to appear with a higher signal than its neighbor with a higher activity concentration. The construction of the storage phosphor detector tip assumed a cylindrical shape for the coronary artery which in reality may have a complicated shape also varying the distance of the artery wall from the surface of the detector.

The leading cause of acute ischaemic syndrome is the rupture of plaques that are not large enough to cause severe stenosis [21]. The storage phosphor detector tip is a potential solution to this generational disease by providing a simple, inexpensive and informative method for the imaging of the sites of increased metabolic activity throughout the entire length of the coronary artery.

REFERENCES

1. World Health Organization 2004 *Cardiovascular Diseases Program-Prevention and Control*

2. Castelli, W.P., *The new pathophysiology of coronary artery disease.* Am J Cardiol, 1998. 82(10B): p. 60T-65T.

3. Burke, A.P., et al., *Coronary risk factors and plaque morphology in men with coronary disease who died suddenly.* New England Journal of Medicine, 1997. 336(18): p. 1276-1282.

4. Tearney, G.J., et al., *Quantification of macrophage content in atherosclerotic plaques by optical coherence tomography.* Circulation, 2003. 107(1): p. 113-119.

5. Toth, P.P., *Subclinical atherosclerosis: what it is, what it means and what we can do about it.* International Journal of Clinical Practice, 2008. 62(8): p. 1246-1254.

6. Fink, L.M., et al., *Elevated serum homocysteine is associated with extent of coronary artery atherosclerosis at autopsy, but is not a risk factor for sudden coronary death.* Blood, 1997. 90(10): p. 3040-3040.

7. Shikhaliev, P.M., et al., *Positron autoradiography for intravascular imaging: feasibility evaluation.* Phys Med Biol, 2006. 51(4): p. 963-79.

8. Cherry, S.R., J.A. Sorenson, and M.E. Phelps, *Physics in nuclear medicine*. 3rd ed. 2003, Philadelphia, PA: Saunders. xiii, 523 p.

9. Bushberg, J.T., *The essential physics of medical imaging*. 2nd ed. 2002, Philadelphia: Lippincott Williams & Wilkins. xvi, 933 p.

10. Sugawara, Y., et al., *Rapid detection of human infections with fluorine-18 fluorodeoxyglucose and positron emission tomography: preliminary results.* European Journal of Nuclear Medicine, 1998. 25(9): p. 1238-1243.

11. Tobis, J.M., et al., *Intravascular Ultrasound Imaging of Human Coronary-Arteries Invivo - Analysis of Tissue Characterizations with Comparison to Invitro Histological Specimens.* Circulation, 1991. 83(3): p. 913-926.

12. Correia, L.C., et al., *Intravascular magnetic resonance imaging of aortic atherosclerotic plaque composition.* Arterioscler Thromb Vasc Biol, 1997. 17(12): p. 3626-32.

13. Zimmermann-Paul, G.G., et al., *High-resolution intravascular magnetic resonance imaging: monitoring of plaque formation in heritable hyperlipidemic rabbits.* Circulation, 1999. 99(8): p. 1054-61.

14. Rudd, J.H.F., et al., *Imaging atherosclerotic plaque inflammation with [F-18]-fluorodeoxyglucose positron emission tomography.* Circulation, 2002. 105(23): p. 2708-2711.

15. Yamaguchi, Y., et al., *Performance of Intravascular Probe in Animal Studies.* IEEE, 2003. 4: p. 2463-7.

16. Janecek, M., et al., *Multi-element linear array of silicon detectors for imaging beta emitting compounds in the coronary arteries.* Nuclear Science Symposium Conference Record, 2002 IEEE (10-16 Nov. 2002), 2002. 3: p. 1416-9.

17. Burgess, A.E., *The Rose model, revisited.* J Opt Soc Am A Opt Image Sci Vis, 1999. 16(3): p. 633-46.

18. Rose, A., *The Sensitivity Performance of the Human Eye on an Absolute Scale.* Journal of the Optical Society of America, 1948. 38(2): p. 196-208.

19. Hillen, W., U. Schiebel, and T. Zaengel, *Imaging performance of a digital storage phosphor system.* Med Phys, 1987. 14(5): p. 744-51.

20. Knoll, G.F., *Radiation detection and measurement*. 3rd ed. 2000, New York: Wiley. xiv, 802 p.

21. Levin, C.S. and E.J. Hoffman, *Calculation of positron range and its effect on the fundamental limit of positron emission tomography system spatial resolution.* Phys Med Biol, 1999. 44(3): p. 781-99.

22. Shah, P.K., *Mechanisms of plaque vulnerability and rupture.* Journal of the American College of Cardiology, 2003. 41(4): p. 15s-22s.

VITA

Peter Petrek was born in Kralovsky Chlmec, Slovakia, in June 1985, son of Steven and Rose Petrek. He graduated from Gymnazium Kralovsky Chlmec High School in 2003, and went on to attend the Augustana College where he studied physics. There he became a member of both, Sigma Pi Sigma and Phi Beta Kappa, Physics and Academic honor societies. Upon receiving his bachelor's degree in physics in 2007, Peter attended Louisiana State University to study medical physics in the Department of Physics and Astronomy. Since then, he has been enrolled in the Graduate School at Louisiana State University and is a candidate for the master's degree in medical physics.